



Supplement of

Evaluation of hydrological models on small mountainous catchments: impact of the meteorological forcings

Guillaume Evin et al.

Correspondence to: Guillaume Evin (guillaume.evin@inrae.fr)

The copyright of individual parts of the supplement might differ from the article licence.

S1 Characteristics of the 55 catchments

Table S1. Characteristics of the 55 catchments: Number; Name (river and outlet); Area (km^2); Median elevation (m); Minimum elevation (m); Maximum elevation (m); Percentage of the catchment covered by ice; Percentage of the catchment characterized as karstic or supplying karstic sources.

Number	Name	Area	Med. elev.	Min. elev.	Max. elev.	%ice	%karst
1	LeRedon@Margencel	30	605	409	1519	0	21
2	LeForon@Sciez	59	569	387	1451	0	0
3	LaDransedeMorzine@Seytroux	172	1424	694	2449	0	5
4	LeRisse@Saint-Jeoire	55	1111	539	1939	0	82
5	L'Arve@Chamonix-Mont-Blanc	201	2510	1020	4187	28	0
6	L'Aire@Saint-Julien-en-Genevois	44	632	436	1380	0	18
7	LesUsses@Musieges	186	663	343	1379	0	16
8	LeBronze@Bonneville	29	1438	455	2335	0	100
9	LaFiliere@Argonay	155	858	488	1997	0	40
10	LeFier@Dingy-Saint-Clair	229	1220	514	2589	0	100
11	LaChaise@Ugine	78	982	429	2380	0	100
12	L'EauMorte@Doussard	92	1059	456	2297	0	100
13	L'Ire@Doussard	27	1241	469	2159	0	100
14	LaBornette@Lathuile	12	1108	467	1882	0	100
15	LeLaudon@Saint-Jorioz	29	928	468	1750	0	100
16	LesEparis@Alby-sur-Cheran	24	645	417	1693	0	31
17	LaNephaz@Rumilly	29	550	326	1008	0	19
18	LeSierroz@Aix-les-Bains	133	521	245	1556	0	23
19	LeCheran@Alleves	261	1149	577	2194	0	100
20	LaLeysse@laRavoire	95	1065	301	1828	0	100
21	LeTillet@Aix-les-Bains	33	352	251	1502	0	20
22	L'Albane@Chambery	47	466	279	1550	0	100
23	L'Hyeres@Chambery	84	683	264	1668	0	73
24	LaLeysse@laMotte-Servolex	289	684	239	1828	0	80
25	LeFlon@Traize	45	593	293	1477	0	29
26	LaLeysse@Nances	28	524	379	1373	0	19
27	LeGuiersVif@Saint-Christophe-sur-Guiers	120	1179	407	2043	0	100
28	LeGuiersMort@Saint-Laurent-du-Pont	92	1232	400	2068	0	98
29	L'Hien@Saint-Victor-de-Cessieu	50	518	352	688	0	0
30	L'Agny@Nivolas-Vermelle	58	498	292	684	0	0
31	LaBourbre@Bourgoin-Jallieu	303	455	246	753	0	0
32	LaVesonne@Estrabilin	173	424	219	602	0	0
33	LaVega@Pont-Eveque	81	297	174	423	0	0
34	LaSanne@Saint-Romain-de-Surieu	30	380	241	463	0	0
35	LeRival@Brezins	175	490	368	784	0	0
36	LaGalaure@Saint-Uze	233	400	159	724	0	0
37	L'Herbasse@Clerieux	195	362	140	629	0	0
38	LeMeaudret@Meaudre	74	1249	958	1686	0	100
39	LaGresse@Gresse-en-Vercors	24	1401	1116	2325	0	100
40	LaGervanne@Beaufort-sur-Gervanne	104	835	314	1570	0	100
41	LaBarberolle@Barbieres	10	739	437	1286	0	4
42	LaVeore@Beaumont-les-Valence	190	271	126	1238	0	9
43	LaDurance@Val-des-Pres	193	2291	1361	3082	0	0
44	LaGuisane@LeMonetier-les-Bains	82	2399	1517	3601	2	0
45	L'Arvan@Saint-Jean-d'Arves	57	2027	1360	3440	4	0
46	LeGelon@laRochette	63	1013	330	2454	0	0
47	LaRoizonne@laValette	71	1736	935	2848	0	5
48	LaJonche@laMure	47	1038	876	2290	0	77
49	LaBonne@Entraigues	142	1952	778	3540	0	7
50	LaSeveraisse@Villar-Loubiere	130	2182	1020	3633	1	0
51	LaSoulouise@Saint-Etienne-en-Devoluy	39	1770	1262	2620	0	0
52	LaRibiere@Agnieres-en-Devoluy	24	1683	1252	2587	0	1
53	LeBez@Chatillon-en-Diois	225	1234	559	2029	0	100
54	LaDrome@Luc-en-Diois	197	1000	540	1712	0	99
55	LaMorge@Voiron	46	532	268	942	0	14

S2 Disaggregation from daily to hourly precipitation and temperature using the method of fragments

S2.1 Precipitation

For a day d , let P_d denote the daily SPAZM precipitation at a pixel that we want to disaggregate. The method of fragments (Wójcik and Buishand, 2003; Breinl and Di Baldassarre, 2019) consists in using the temporal structure of another precipitation data available at a finer scale and preserving the daily amounts. Let \tilde{P}_h denote the hourly precipitation for this alternative source, where $h = 1, \dots, 24$ corresponds to the day d , and $\tilde{P}_d = \sum_h \tilde{P}_h$ is the corresponding daily amount. If \tilde{P}_d greater than zero positive at this pixel, then the disaggregated hourly amounts P_h are obtained as follows:

$$P_h = \tilde{P}_h \times \frac{\tilde{P}_d}{P_d}. \quad (\text{S1})$$

Obviously, when $P_d = 0$, there is no precipitation to disaggregate and P_h equals zero for any hour h of the day. However, when P_d is positive and \tilde{P}_d is equal to zero, the temporal structure \tilde{P}_d is absent and different solutions have been considered:

- **SPAZM-c:** COMEPHORE data are used to provide the finer precipitation data \tilde{P} . However, if for a day d and some pixels, $\tilde{P}_d = 0$, then we look for hourly gauged precipitation data for the same day d in the neighbouring region of these pixels, at a maximum distance of 100 km. If no precipitation data can be found inside this circle with a 100 km radius, \tilde{P} is uniformly distributed throughout the day.
- **SPAZM-g:** This second approach is similar to SPAZM-c, except that COMEPHORE data are not used to disaggregate SPAZM precipitation, i.e. only gauged precipitation data close to the pixels are used.

S2.2 Temperature

Similarly to SPAZM precipitation, daily SPAZM temperature data are disaggregated to an hourly scale using SAFRAN data as a reference. The daily ranges of SAFRAN temperatures, available at a coarser spatial scale, are corrected using the minimum and maximum daily temperature provided by the SPAZM reanalysis. For a day d and a SPAZM pixel k , the disaggregated temperatures T_h are obtained as follows:

$$T_h = (\tilde{T}_h - \tilde{T}_h^{min}) \times \frac{T_d^{max} - T_d^{min}}{\tilde{T}_d^{max} - \tilde{T}_d^{min}} + T_d^{min}, \quad (\text{S2})$$

where T_d^{min} and T_d^{max} are the daily minimum and maximum SPAZM temperatures, respectively, for the pixel k and the day d , and \tilde{T}_d^{min} and \tilde{T}_d^{max} are minimum and maximum SAFRAN temperatures for this day d and the closest SAFRAN pixel, derived from the hourly SAFRAN temperatures \tilde{T}_h . The daily temperature range produced by SPAZM is thus preserved, and SAFRAN provides the subdaily temporal structure.

S3 Description of the SMASH model structure

The proposed SMASH structure for distributed modeling, based on GR lumped models (Perrin et al., 2003; Valéry, 2010) and schematized in Fig. S1, is composed of 5 reservoirs \mathcal{S} , \mathcal{P} , \mathcal{T}_{ft} , \mathcal{T}_{st} and \mathcal{R} of respective states h_s , h_p , h_{ft} , h_{st} and h_r considered for simulating respectively the snow melt (CemaNeige Valéry, 2010), the production of runoff (GR4, Perrin et al., 2003), and two intermediary reservoirs (linear reservoir with leakage at exponent 5 in the differential model, Jay-Allemand et al. 2020 from GR Perrin et al. 2003) within a given cell x and the routing between cells (linear reservoir). We denote the maximum capacity of the production and transfer reservoirs by c_p , c_{ft} and c_{st} respectively (snow \mathcal{S} and routing \mathcal{R} reservoirs have no maximum capacity).

As no solid/snow precipitation is considered as input, the initial total precipitation P is divided into a liquid part named P_l and a solid part N using a liquid ratio computed as a function of temperature following the S-shaped parametric curve method derived from the MORDOR-SD snow module proposed by Garavaglia et al. (2017). This solid part N is stored in the snow reservoir \mathcal{S} whose melt N_m is a function of temperature, of an estimation of the snow cover area, and of the two parameters of the snow module: tc , the weighting coefficient for the thermal state of the snowpack and mc , the melting coefficient. The evapotranspiration E used as input of the model corresponds to a daily time-series of interannual potential evapotranspiration based on the formula proposed by Oudin et al. (2005), using SAFRAN temperatures, which are disaggregated at an hourly scale using a fixed subdaily distribution.

First, the net rainfall P_n and the net evapotranspiration E_n are obtained from the difference between $P_l + N_m$ and E (i.e. $E_n = 0$ if $E_n \leq P_l + N_m$ and vice versa, see Eqs. 1 and 2 in Jay-Allemand et al., 2020). Then, the partition of P_n between an infiltration part P_s filling the production reservoir \mathcal{P} (soil moisture accounting), and an effective rainfall $P_r = P_n - P_s$ filling the transfer reservoirs is done with a production operator. The production reservoir is then emptied from the actual evaporation E_s . The infiltration P_s and the actual evaporation E_s are functions of P_n and E_n , respectively, c_p and h_p (see Eqs. 3 and 4 in Perrin et al., 2003). The effective rainfall P_r is divided into 10% of direct runoff and 90% of runoff inflowing transfer part with another splitting between the two transfer reservoirs controlled by a partition parameter α . A water exchange term F depending on exc , which is a non-conservative operator, is applied to the direct runoff component and to the first transfer reservoir \mathcal{T}_{ft} (Eq. 18 in Perrin et al., 2003). The total runoff amount Q_t of a cell is therefore the sum of the flows from the direct branch Q_d and the transfer reservoirs Q_{ft} and Q_{st} (Eqs. 20 and 22 in Perrin et al., 2003). Then, the final routed discharge amount Q of a cell is the sum of Q_t and the upstream flow Q_r calculated using a linear routing reservoir \mathcal{R} whose emptying is parameterized by l_r .

The numerical resolution of this ODE-based hydrological model relies on an explicit expression of its solution, approximated on the regular mesh, covering a catchment domain Ω , of constant step dx with a fixed time step dt .

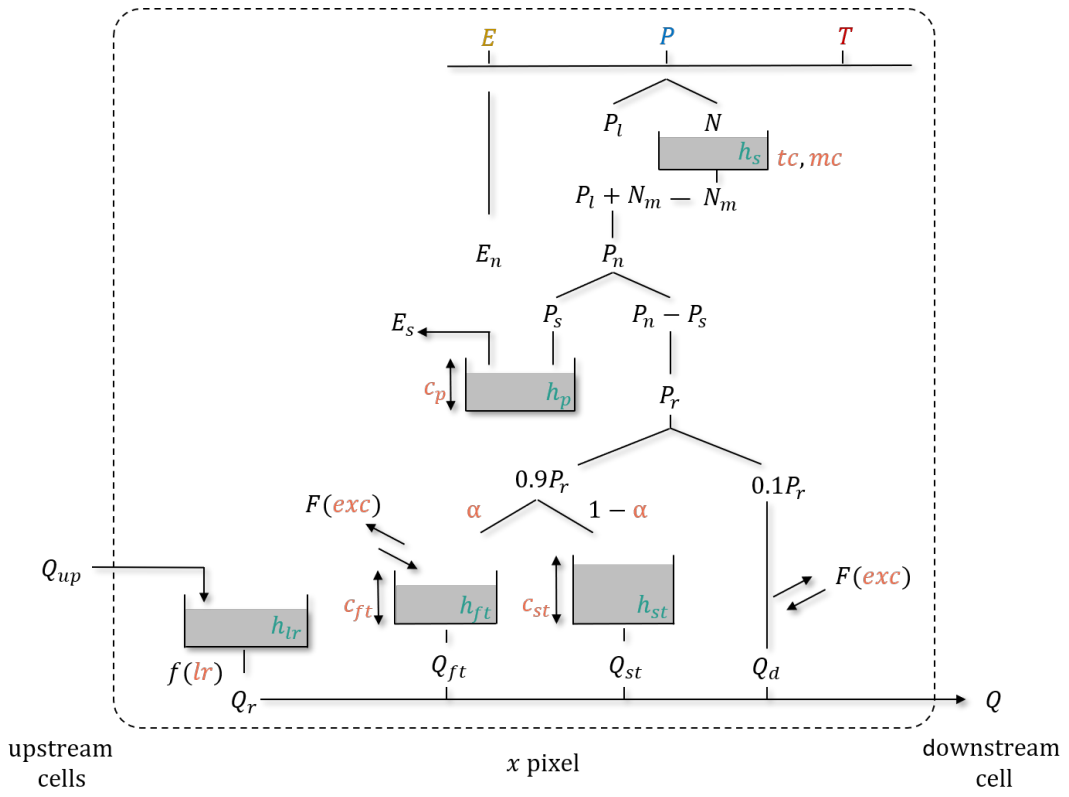


Figure S1. Diagram of the 8-parameter SMASH model.

S4 Percentage of karst

Figure S2 shows the percentage of area characterised as karstic or supplying karstic sources, for each catchment of this study (Brugeron et al., 2018).

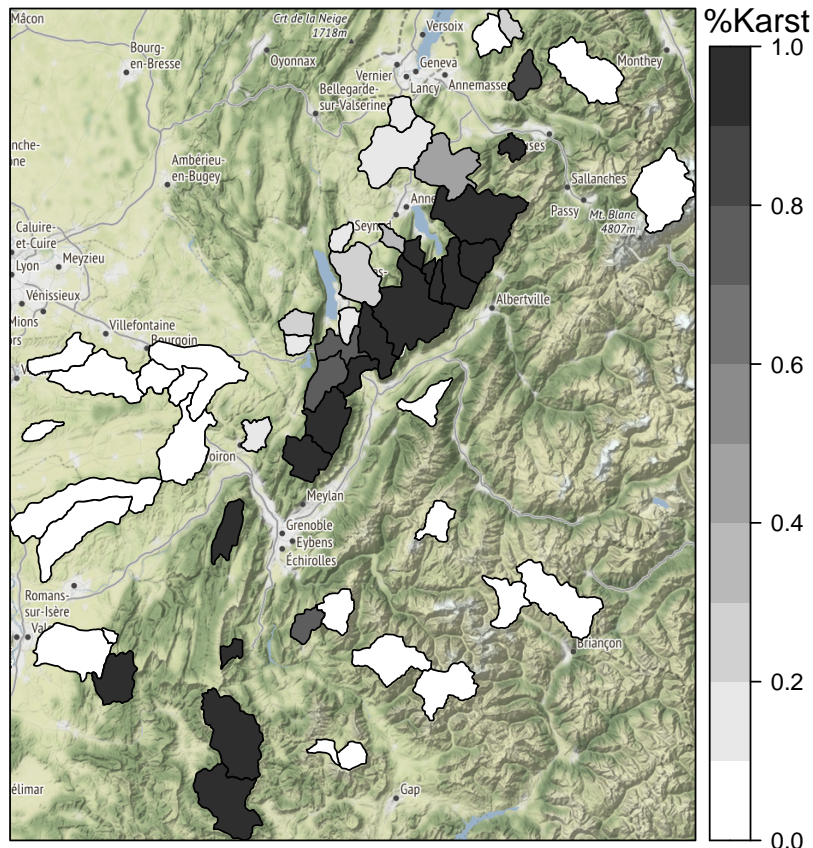


Figure S2. Percentage of karst obtained for each catchment. Map © OpenStreetMap contributors 2023. Distributed under the Open Data Commons Open Database License (ODbL) v1.0

S5 Illustration of large floods

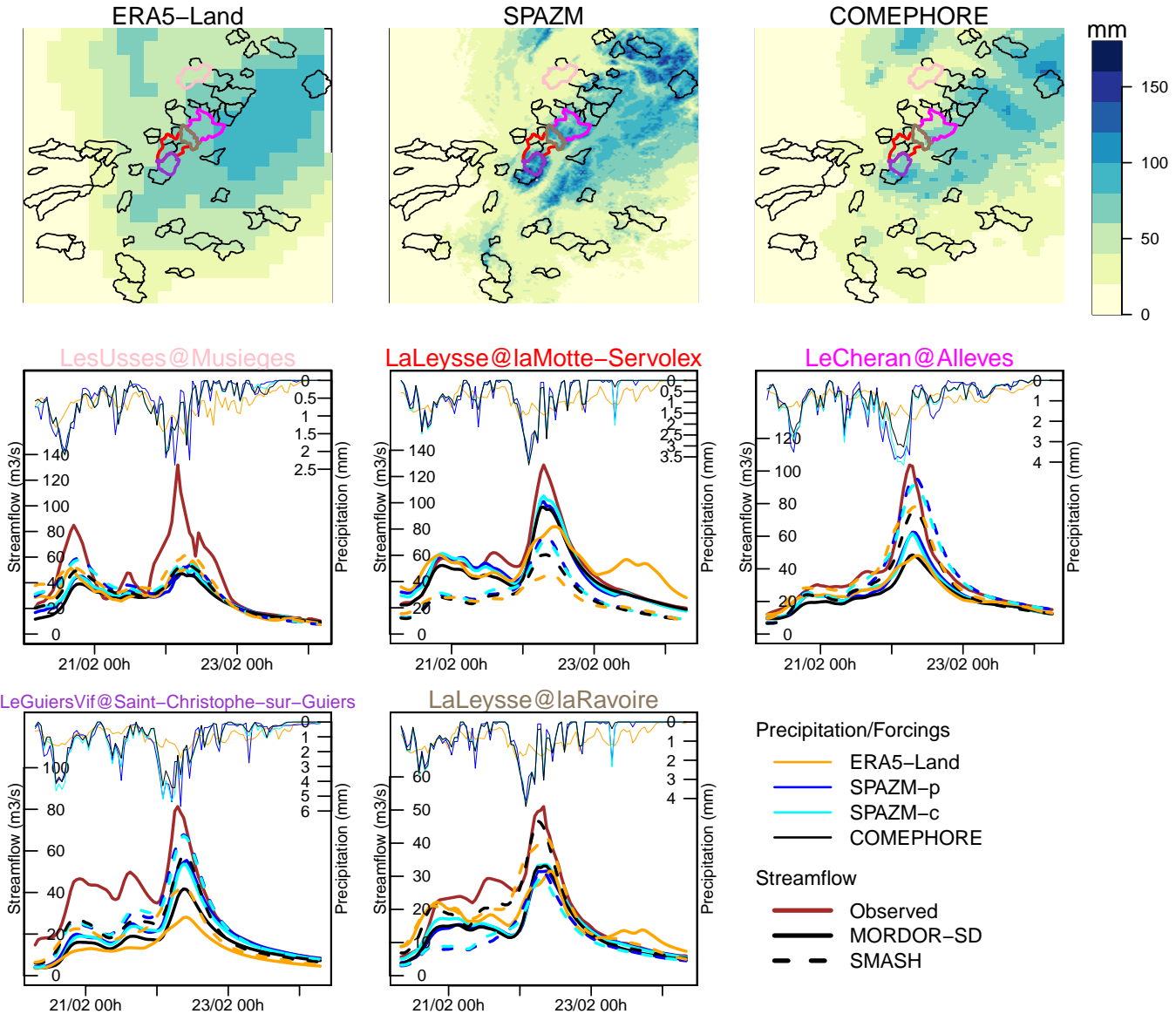


Figure S3. Cumulative amount of precipitation 24 hours before and after 1999-02-22 06:00 for ERA5-Land, SPAZM and COMEPhore (top row) and time series of precipitation (thin lines) and streamflow (thick lines) for five catchments which have reached the highest observed peak flows for this event (middle and bottom rows).

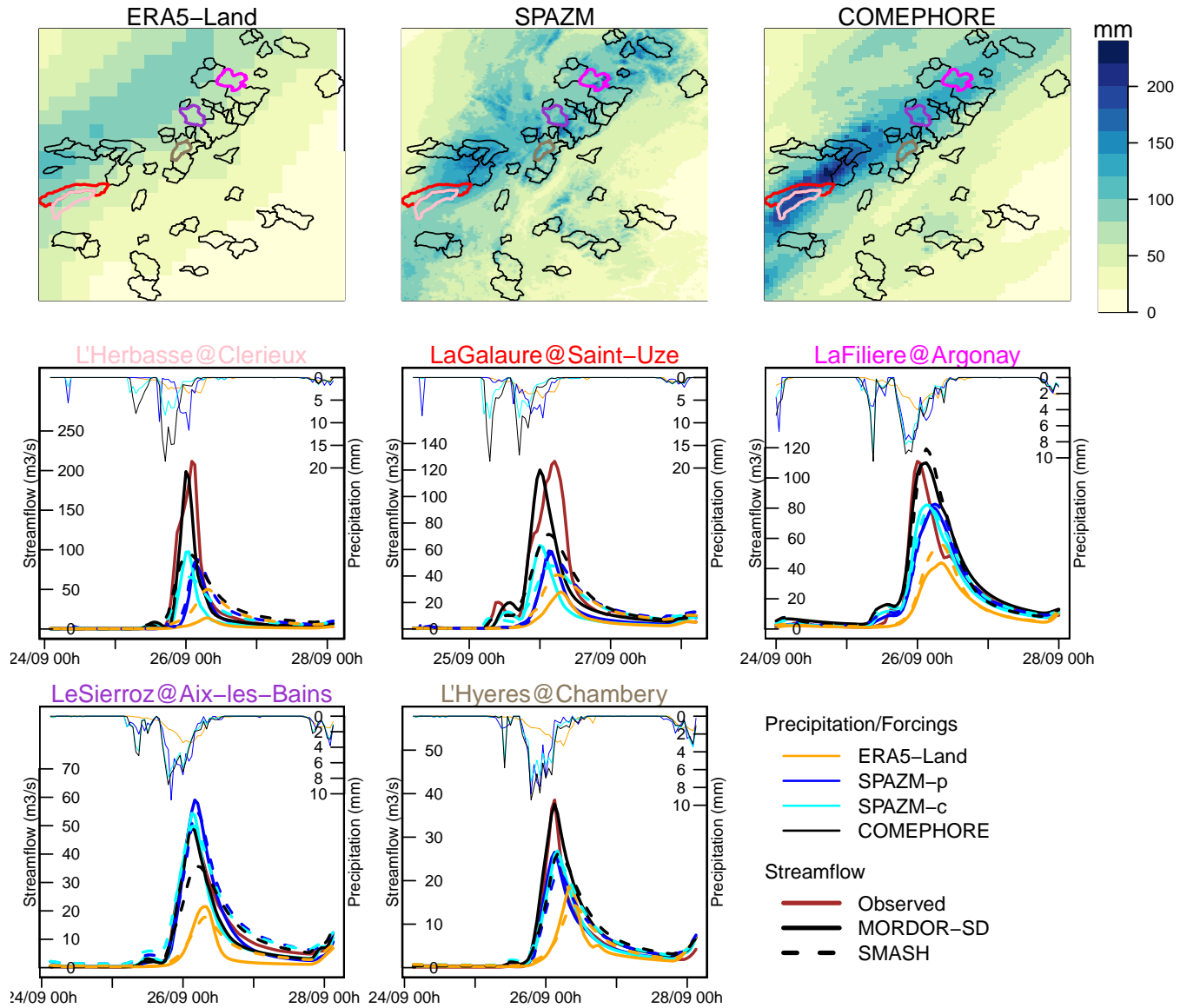


Figure S4. Cumulative amount of precipitation 24 hours before and after 1999-09-26 06:00 for ERA5-Land, SPAZM and COMEPHORE (top row) and time series of precipitation (thin lines) and streamflow (thick lines) for five catchments which have reached the highest observed peak flows for this event (middle and bottom rows).

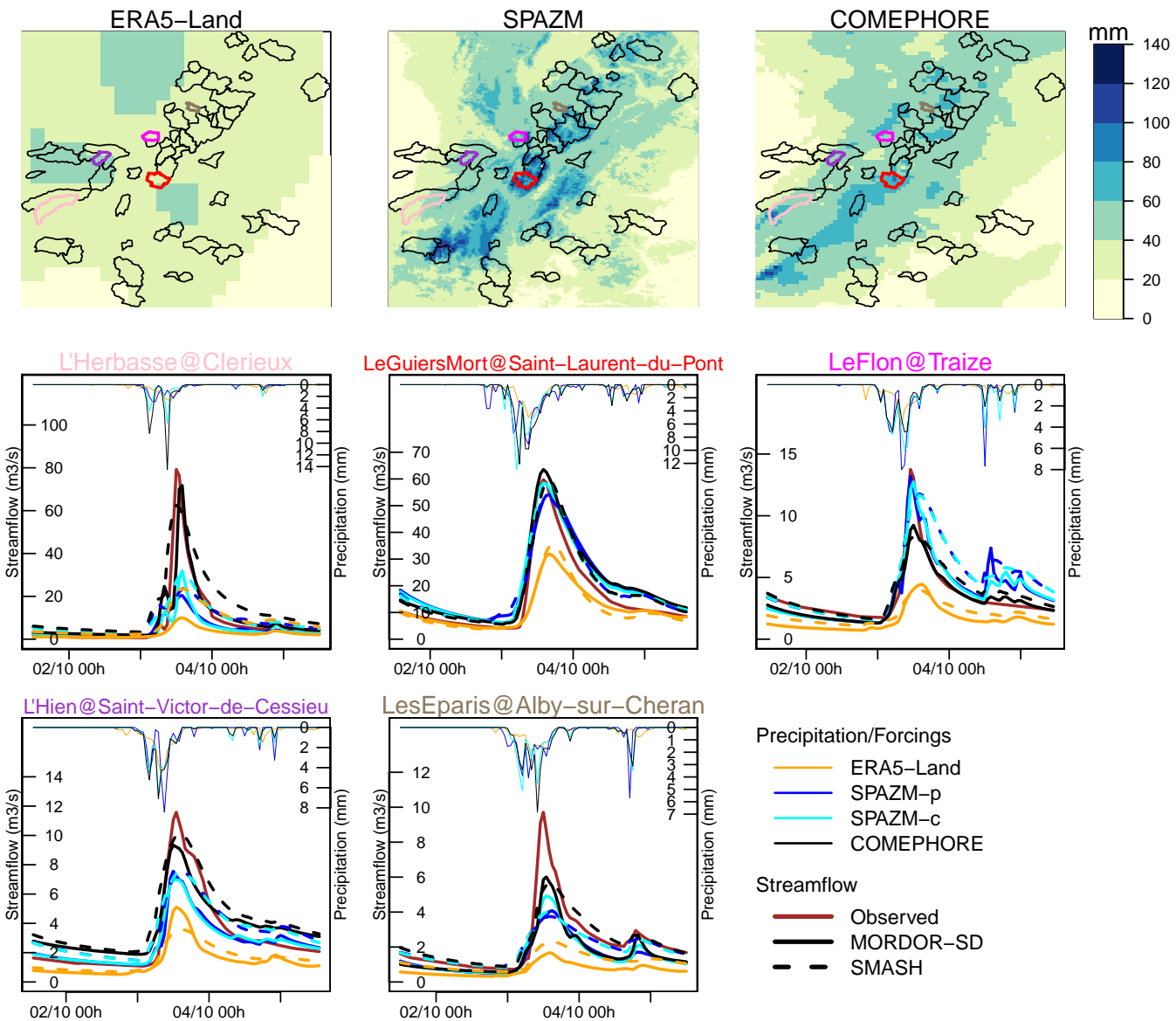


Figure S5. Cumulative amount of precipitation 24 hours before and after 1999-10-03 06:00 for ERA5-Land, SPAZM and COMEPHORE (top row) and time series of precipitation (thin lines) and streamflow (thick lines) for five catchments which have reached the highest observed peak flows for this event (middle and bottom rows).

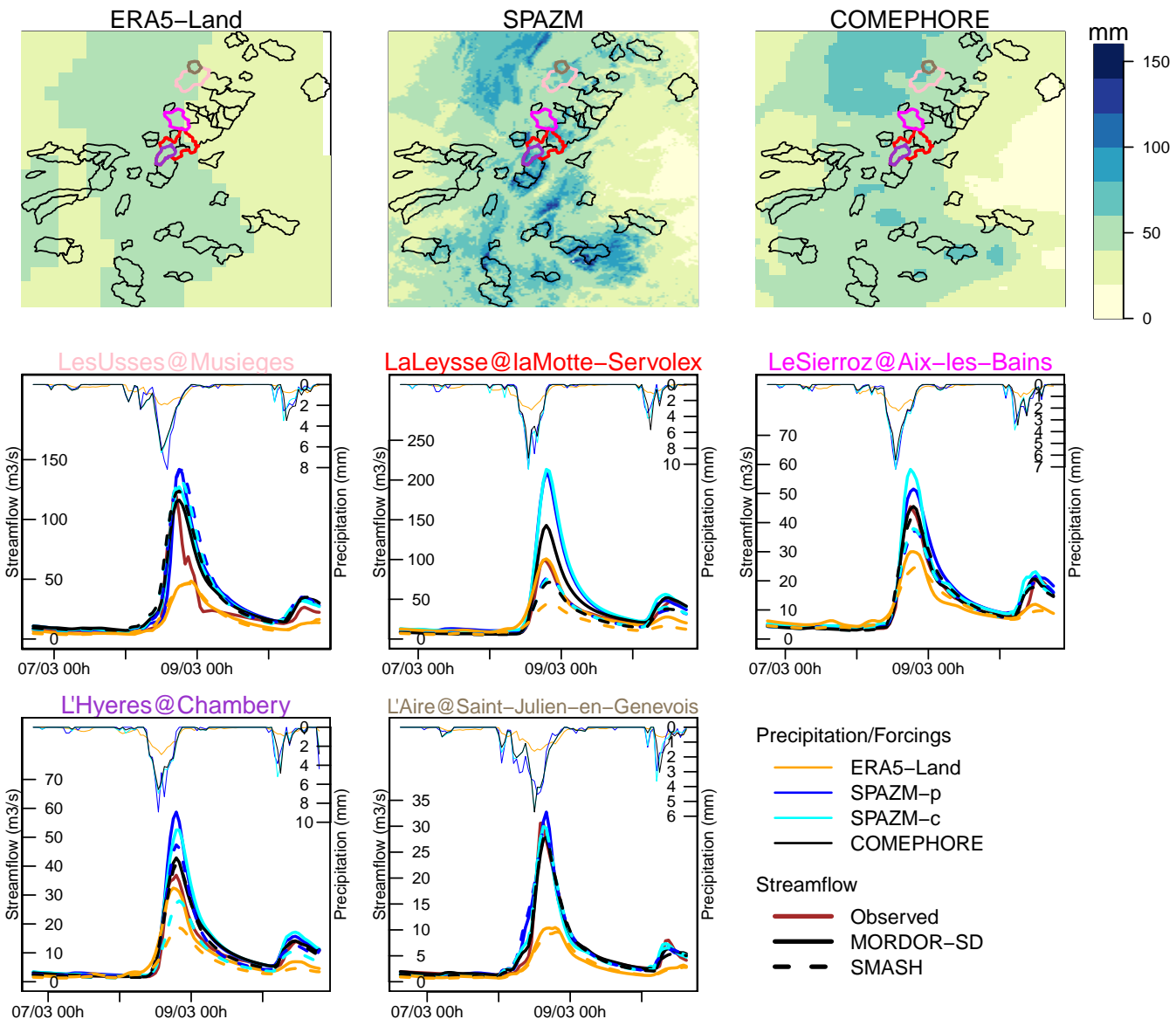


Figure S6. Cumulative amount of precipitation 24 hours before and after 2001-03-08 06:00 for ERA5-Land, SPAZM and COMEPHORE (top row) and time series of precipitation (thin lines) and streamflow (thick lines) for five catchments which have reached the highest observed peak flows for this event (middle and bottom rows).

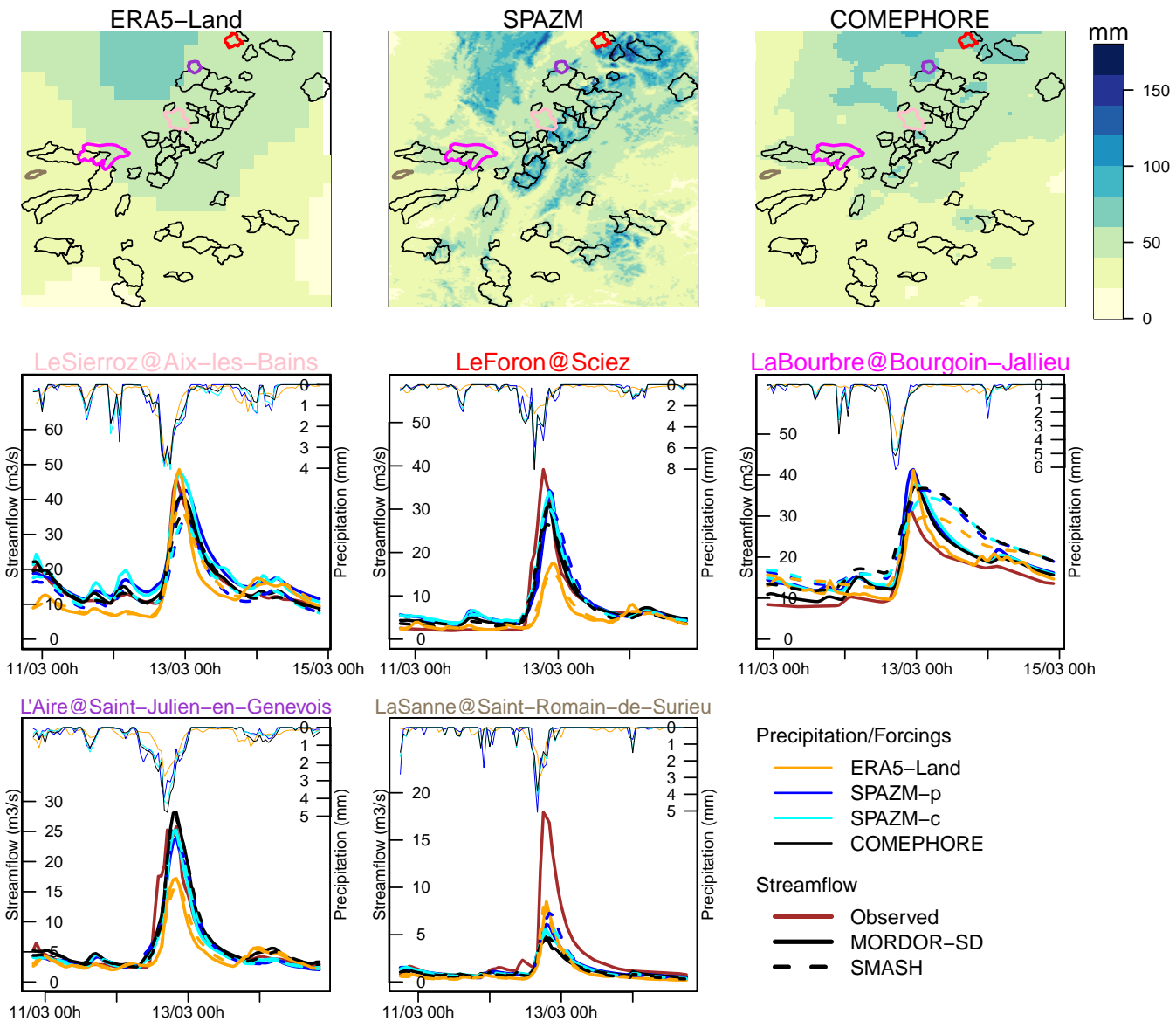


Figure S7. Cumulative amount of precipitation 24 hours before and after 2001-03-12 06:00 for ERA5-Land, SPAZM and COMEPHORE (top row) and time series of precipitation (thin lines) and streamflow (thick lines) for five catchments which have reached the highest observed peak flows for this event (middle and bottom rows).

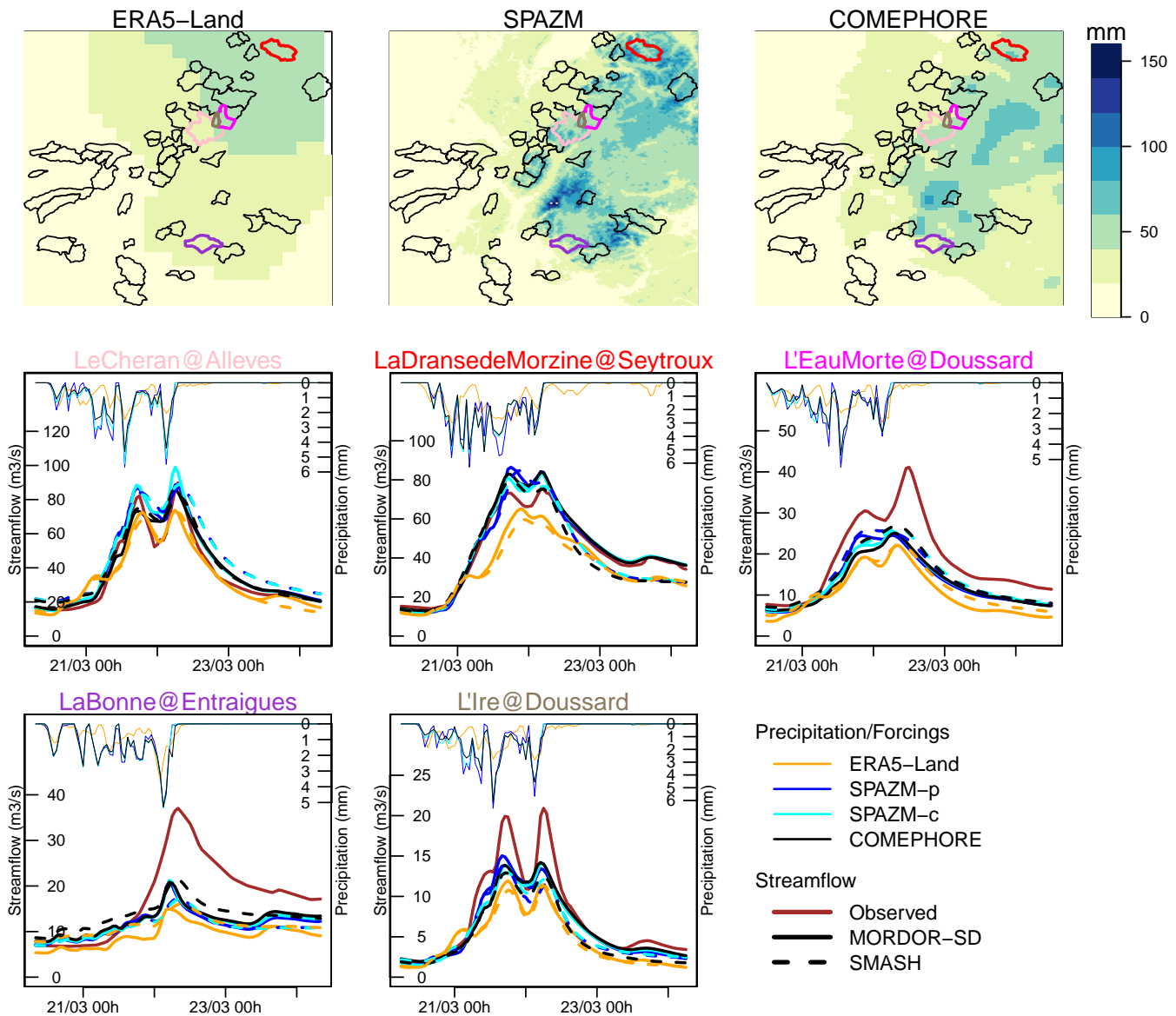


Figure S8. Cumulative amount of precipitation 24 hours before and after 2001-03-22 06:00 for ERA5-Land, SPAZM and COMEPHORE (top row) and time series of precipitation (thin lines) and streamflow (thick lines) for five catchments which have reached the highest observed peak flows for this event (middle and bottom rows).

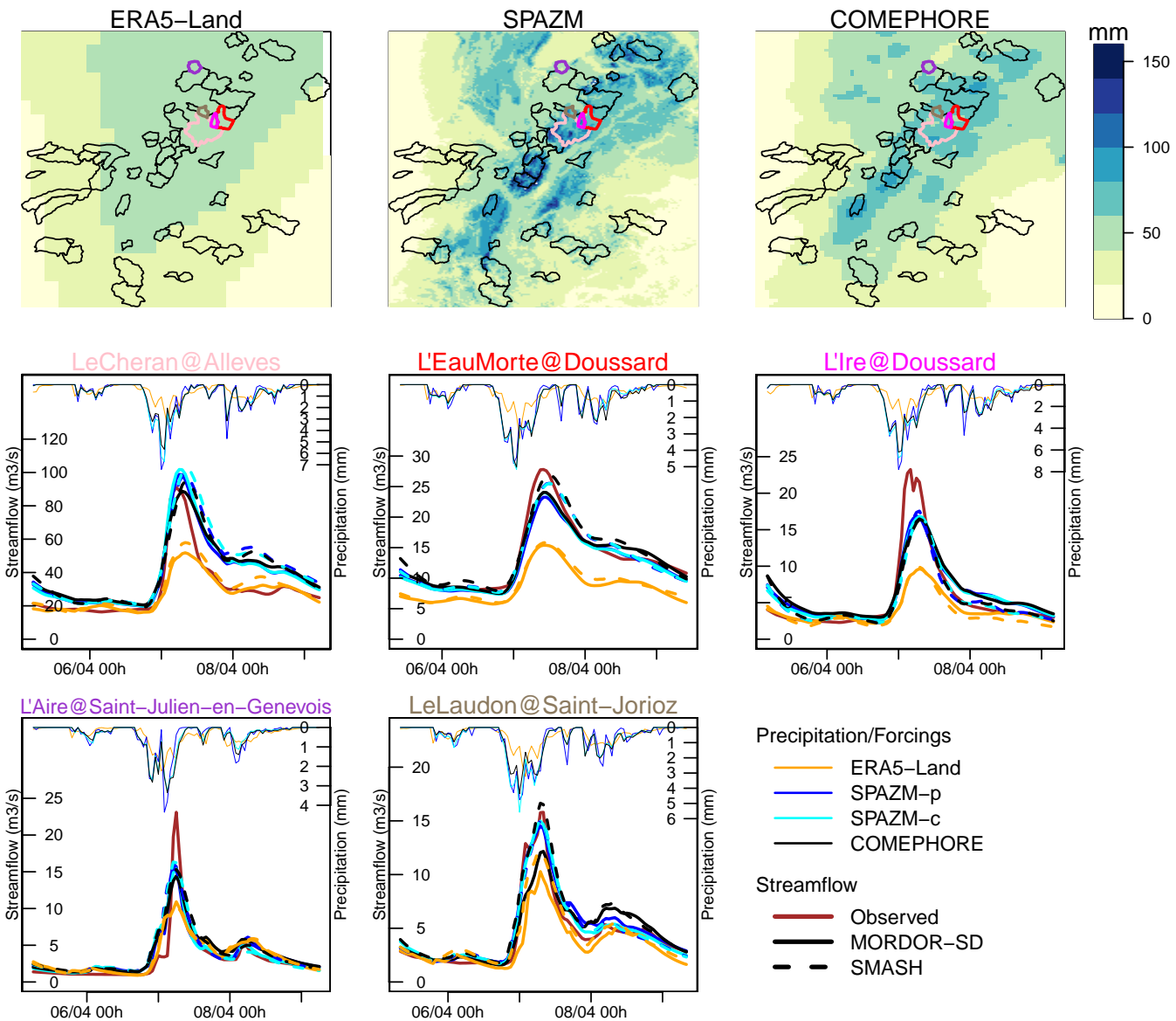


Figure S9. Cumulative amount of precipitation 24 hours before and after 2001-04-07 06:00 for ERA5-Land, SPAZM and COMEPHORE (top row) and time series of precipitation (thin lines) and streamflow (thick lines) for five catchments which have reached the highest observed peak flows for this event (middle and bottom rows).

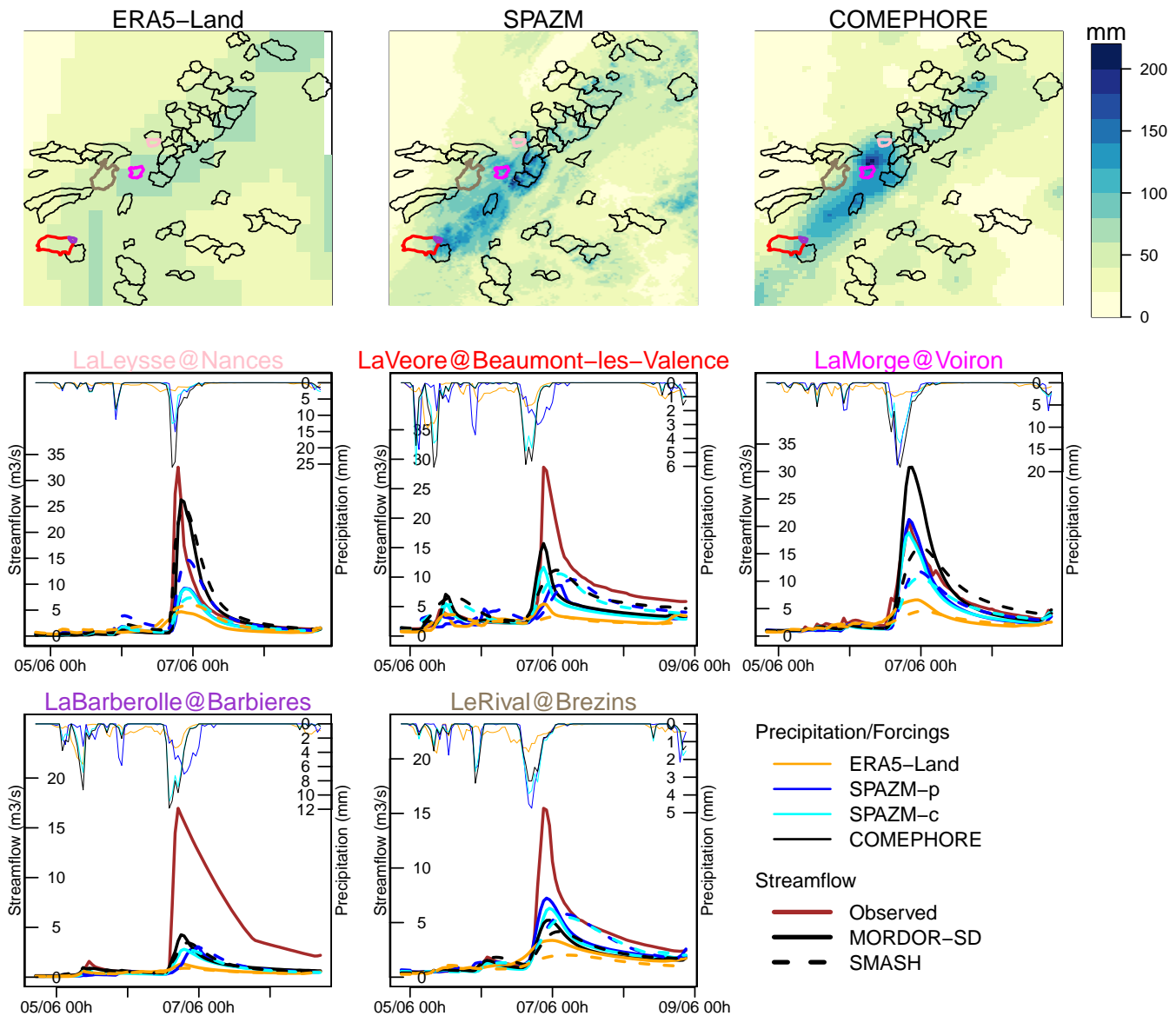


Figure S10. Cumulative amount of precipitation 24 hours before and after 2002-06-06 06:00 for ERA5-Land, SPAZM and COMEPHORE (top row) and time series of precipitation (thin lines) and streamflow (thick lines) for five catchments which have reached the highest observed peak flows for this event (middle and bottom rows).

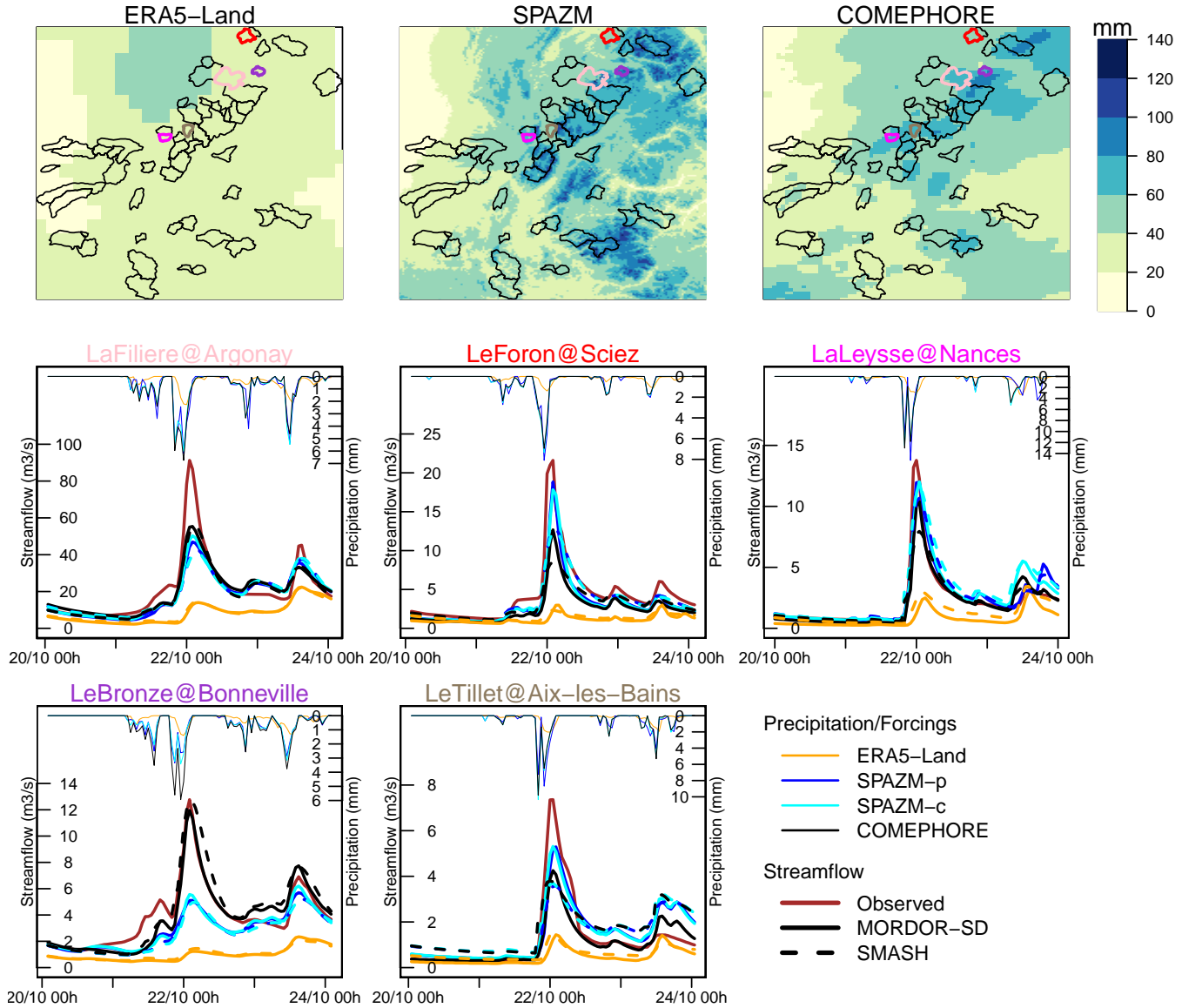


Figure S11. Cumulative amount of precipitation 24 hours before and after 2002-10-22 06:00 for ERA5-Land, SPAZM and COMEPHORE (top row) and time series of precipitation (thin lines) and streamflow (thick lines) for five catchments which have reached the highest observed peak flows for this event (middle and bottom rows).

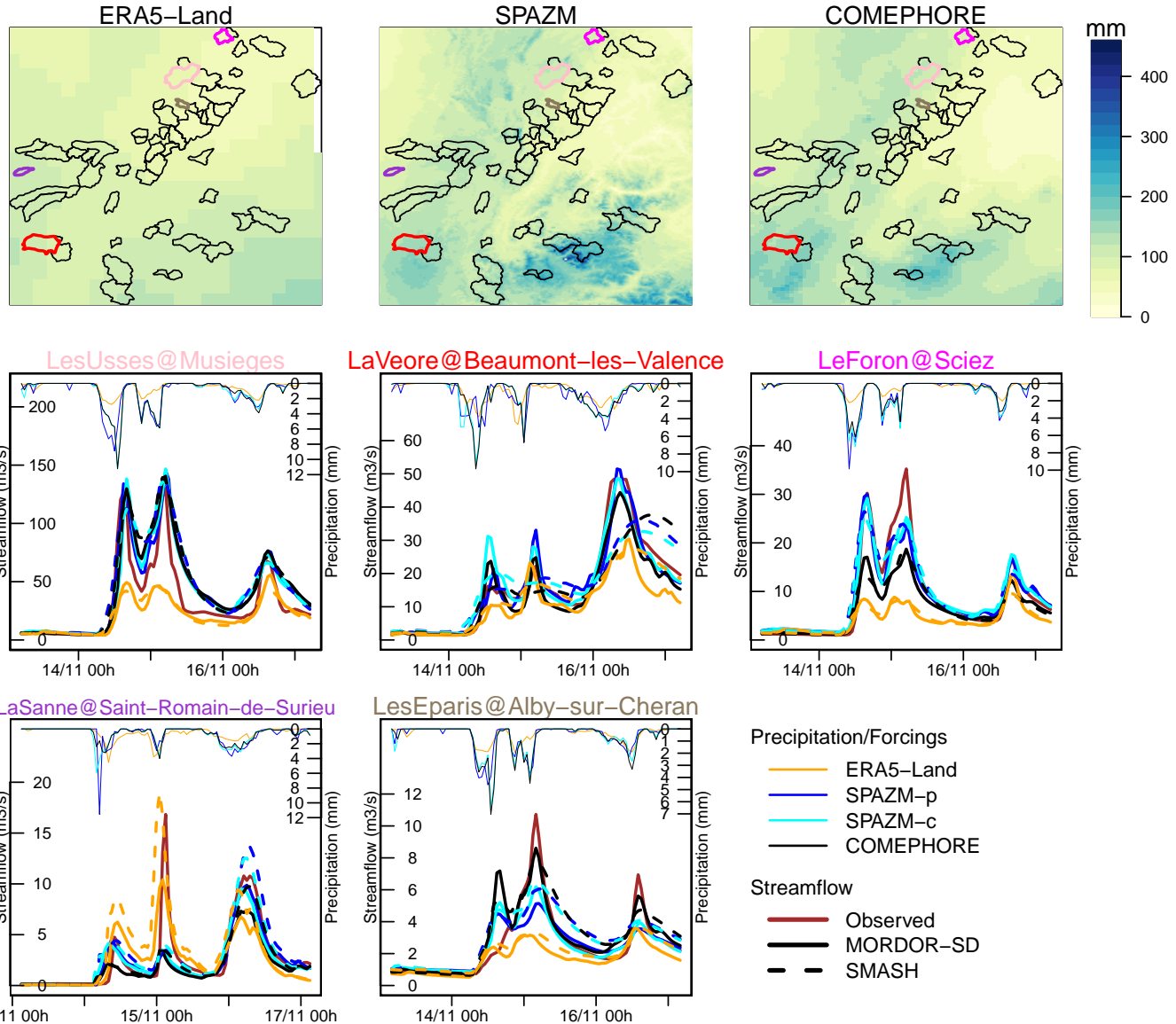


Figure S12. Cumulative amount of precipitation 24 hours before and after 2002-11-15 06:00 for ERA5-Land, SPAZM and COMEPHORE (top row) and time series of precipitation (thin lines) and streamflow (thick lines) for five catchments which have reached the highest observed peak flows for this event (middle and bottom rows).

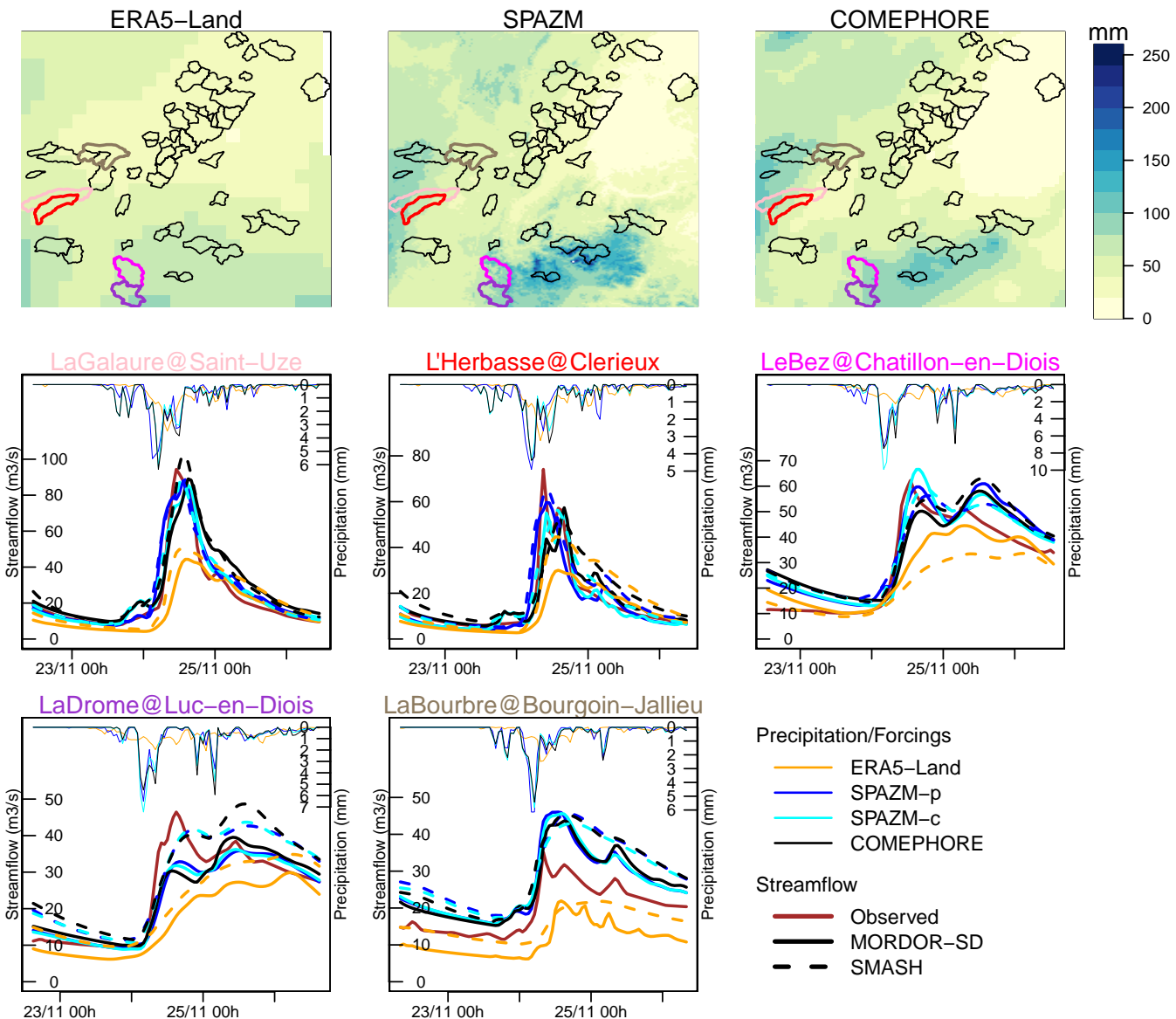


Figure S13. Cumulative amount of precipitation 24 hours before and after 2002-11-24 06:00 for ERA5-Land, SPAZM and COMEPHORE (top row) and time series of precipitation (thin lines) and streamflow (thick lines) for five catchments which have reached the highest observed peak flows for this event (middle and bottom rows).

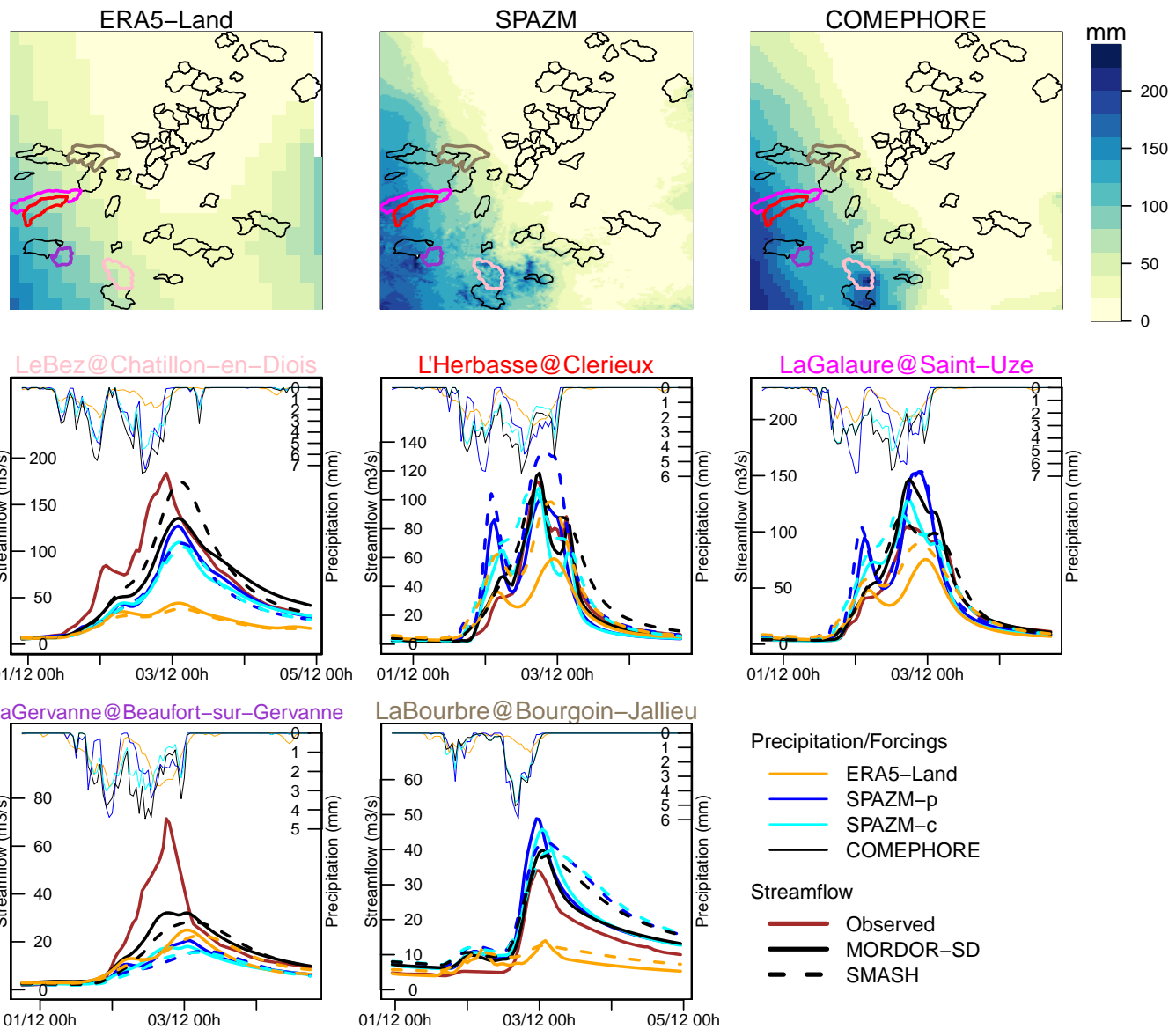


Figure S14. Cumulative amount of precipitation 24 hours before and after 2003-12-02 06:00 for ERA5-Land, SPAZM and COMEPhore (top row) and time series of precipitation (thin lines) and streamflow (thick lines) for five catchments which have reached the highest observed peak flows for this event (middle and bottom rows).

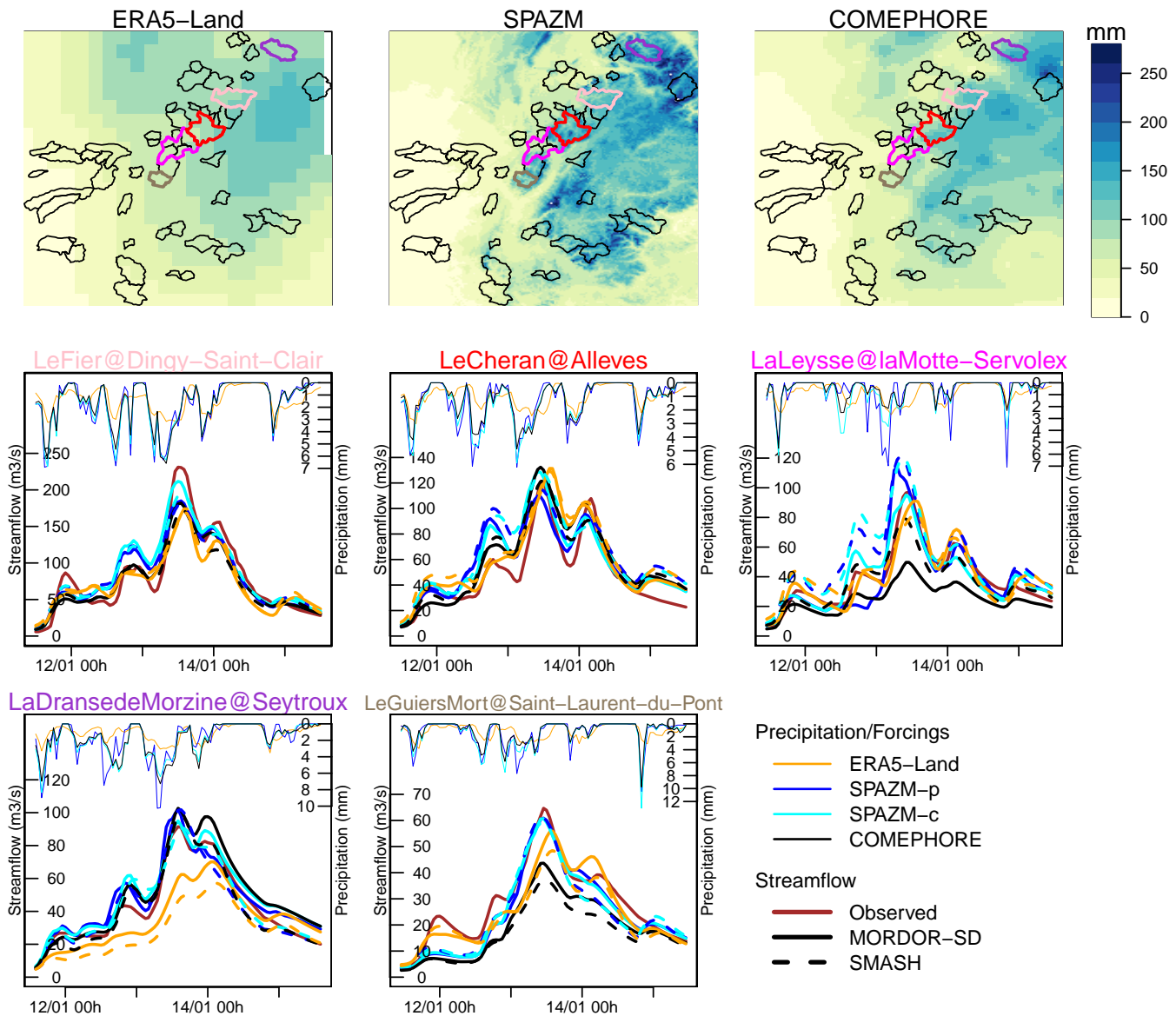


Figure S15. Cumulative amount of precipitation 24 hours before and after 2004-01-13 06:00 for ERA5-Land, SPAZM and COMEPHORE (top row) and time series of precipitation (thin lines) and streamflow (thick lines) for five catchments which have reached the highest observed peak flows for this event (middle and bottom rows).

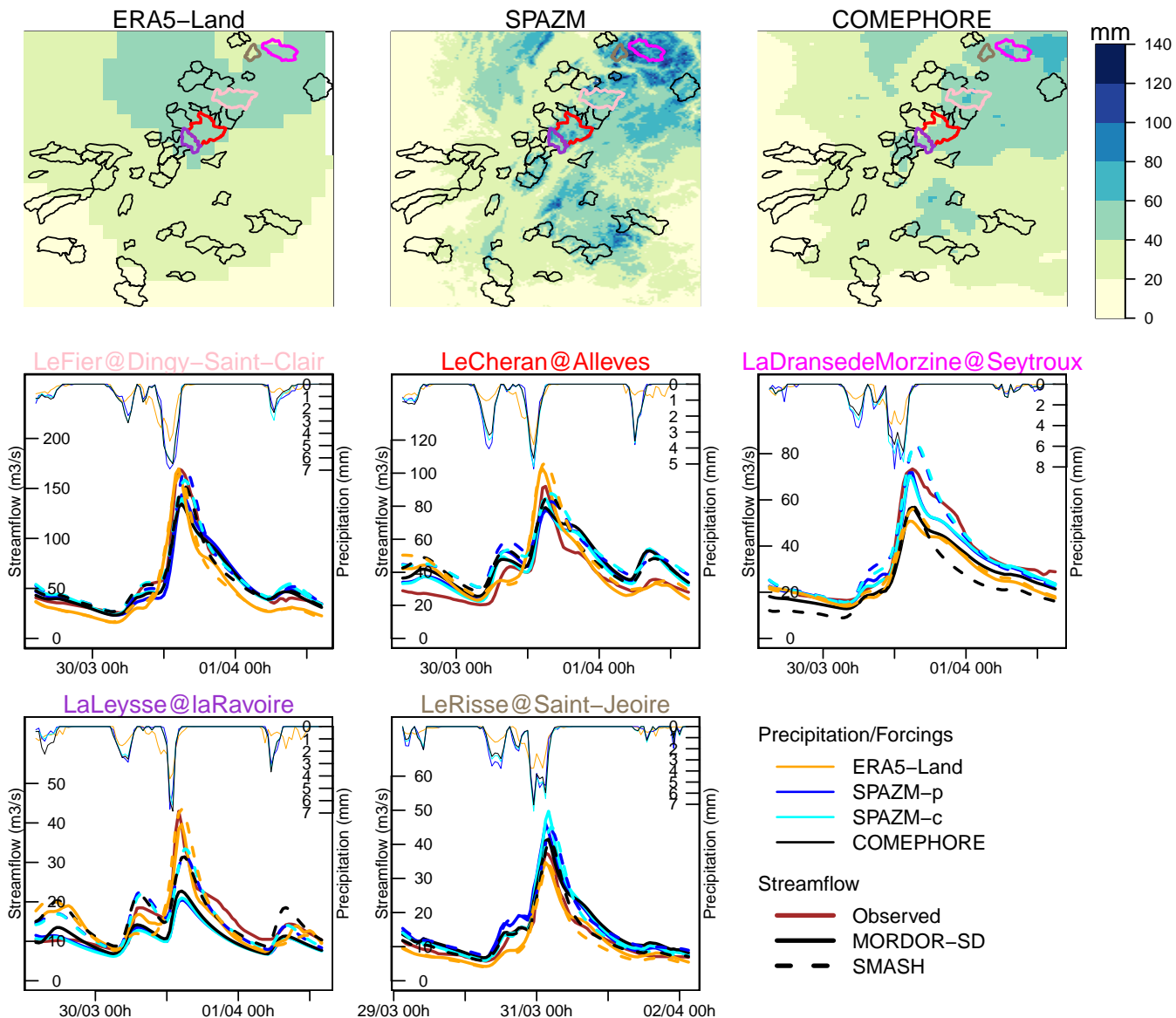


Figure S16. Cumulative amount of precipitation 24 hours before and after 2006-03-31 06:00 for ERA5-Land, SPAZM and COMEPHORE (top row) and time series of precipitation (thin lines) and streamflow (thick lines) for five catchments which have reached the highest observed peak flows for this event (middle and bottom rows).

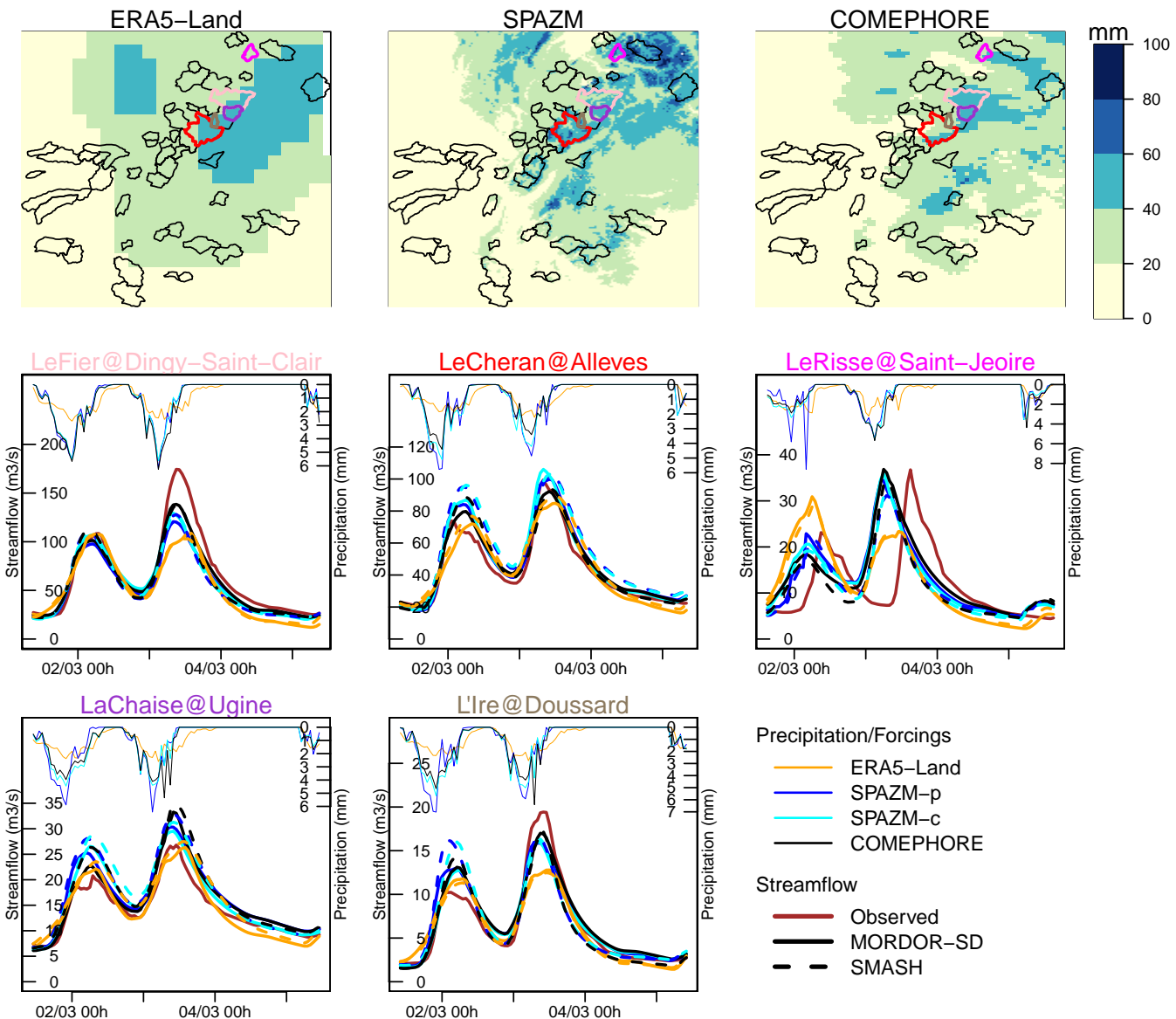


Figure S17. Cumulative amount of precipitation 24 hours before and after 2007-03-03 06:00 for ERA5-Land, SPAZM and COMEPHORE (top row) and time series of precipitation (thin lines) and streamflow (thick lines) for five catchments which have reached the highest observed peak flows for this event (middle and bottom rows).

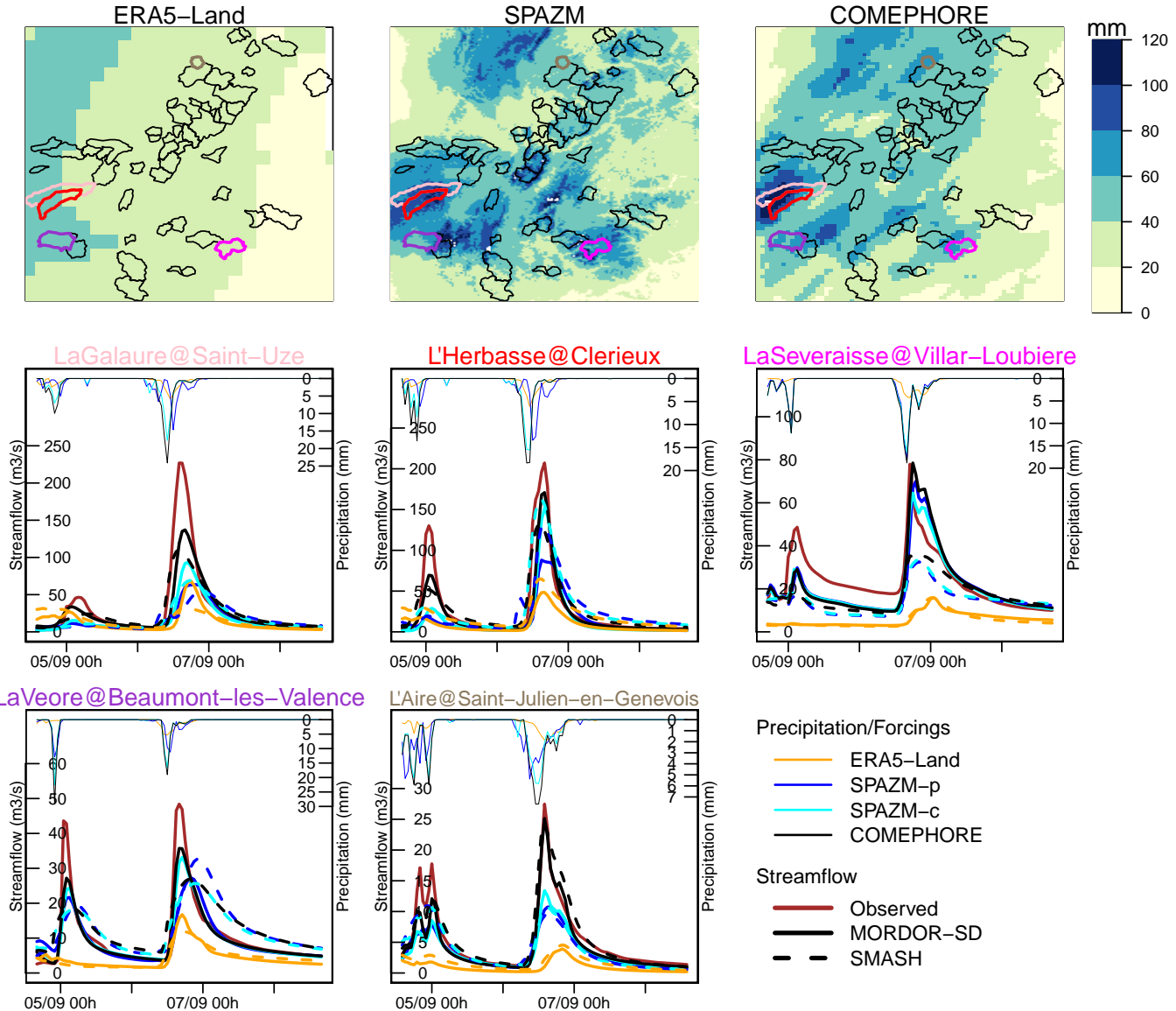


Figure S18. Cumulative amount of precipitation 24 hours before and after 2008-09-06 06:00 for ERA5-Land, SPAZM and COMEPhore (top row) and time series of precipitation (thin lines) and streamflow (thick lines) for five catchments which have reached the highest observed peak flows for this event (middle and bottom rows).

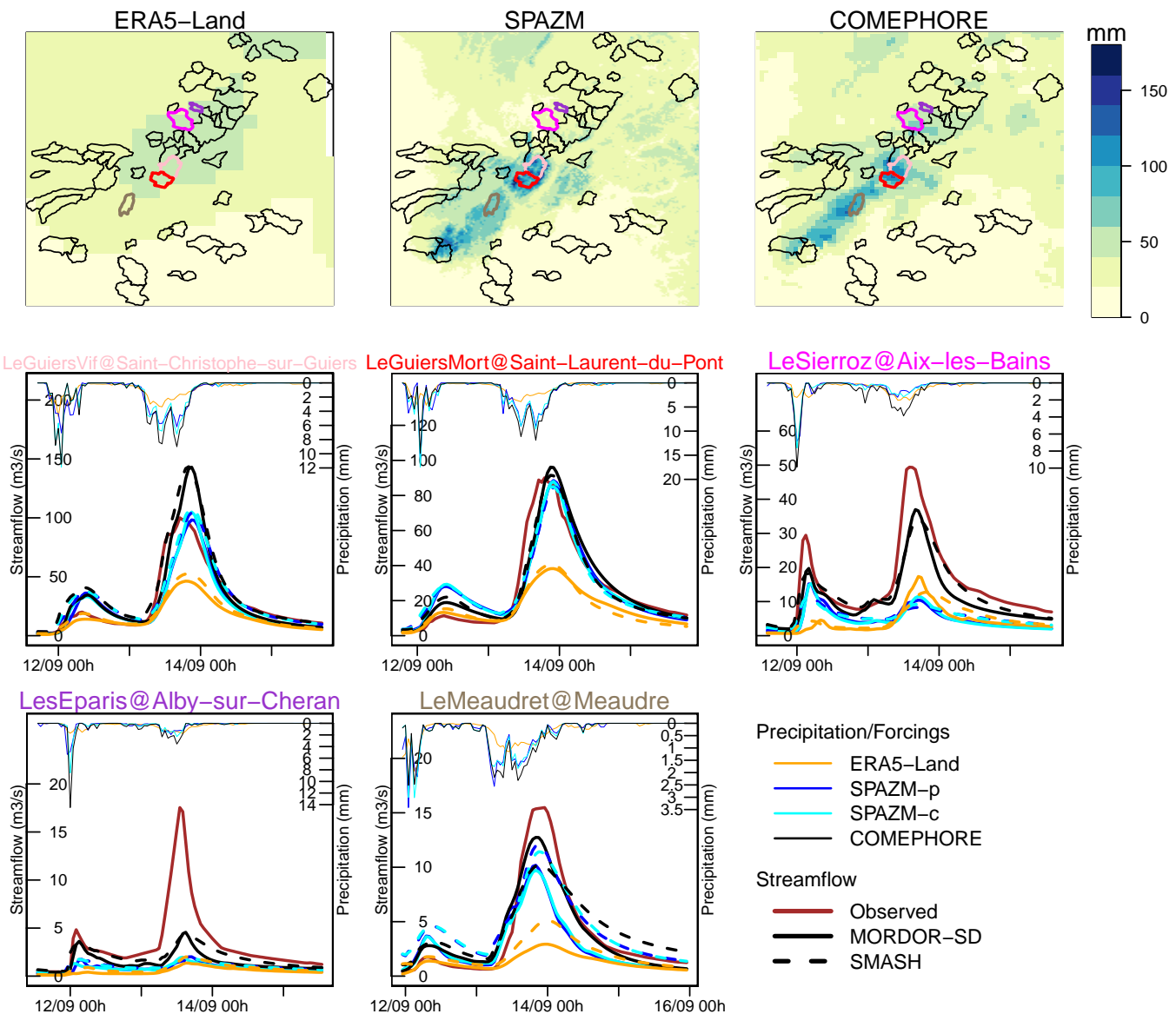


Figure S19. Cumulative amount of precipitation 24 hours before and after 2008-09-13 06:00 for ERA5-Land, SPAZM and COMEPHORE (top row) and time series of precipitation (thin lines) and streamflow (thick lines) for five catchments which have reached the highest observed peak flows for this event (middle and bottom rows).

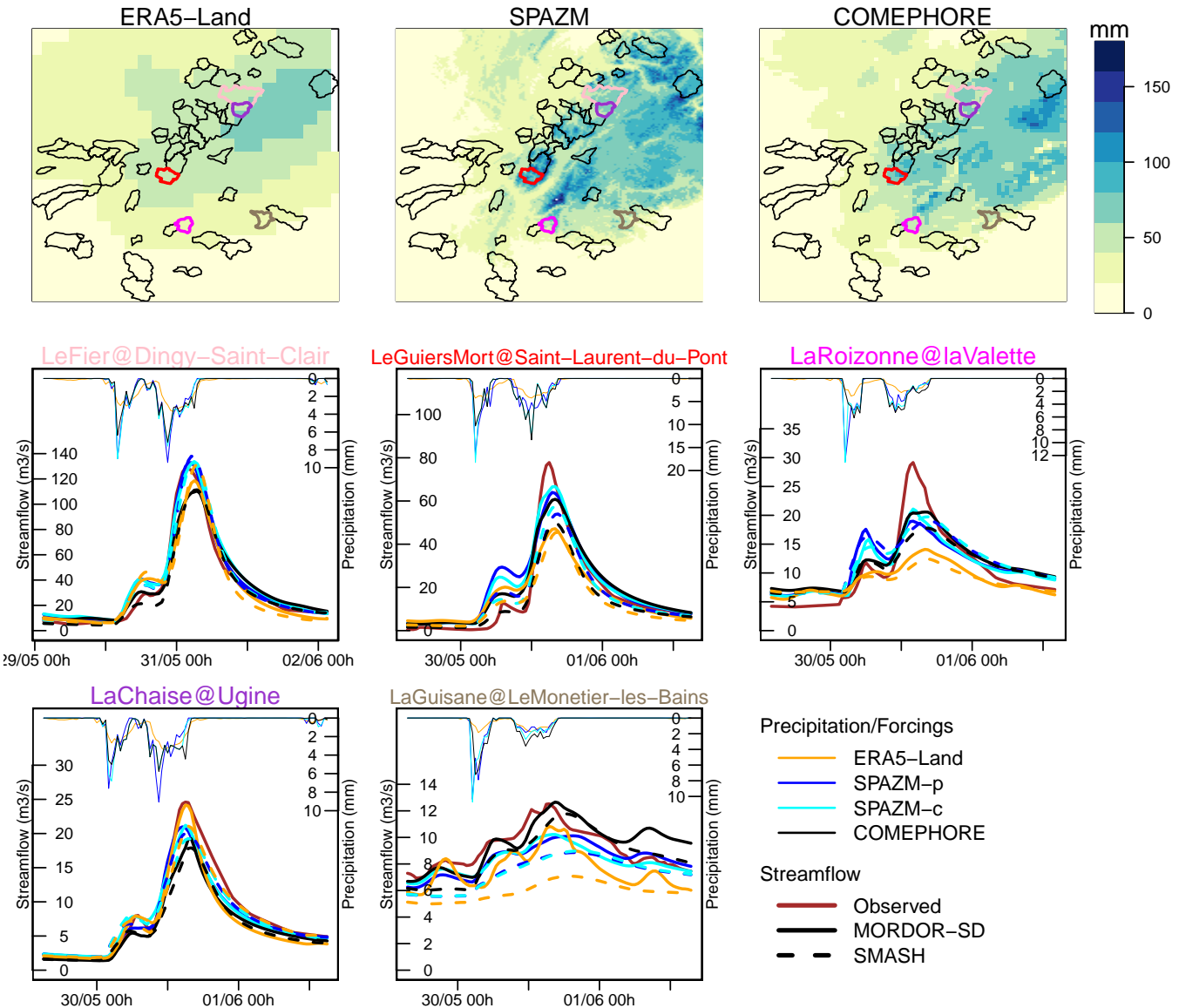


Figure S20. Cumulative amount of precipitation 24 hours before and after 2010-05-31 06:00 for ERA5-Land, SPAZM and COMEPhORE (top row) and time series of precipitation (thin lines) and streamflow (thick lines) for five catchments which have reached the highest observed peak flows for this event (middle and bottom rows).

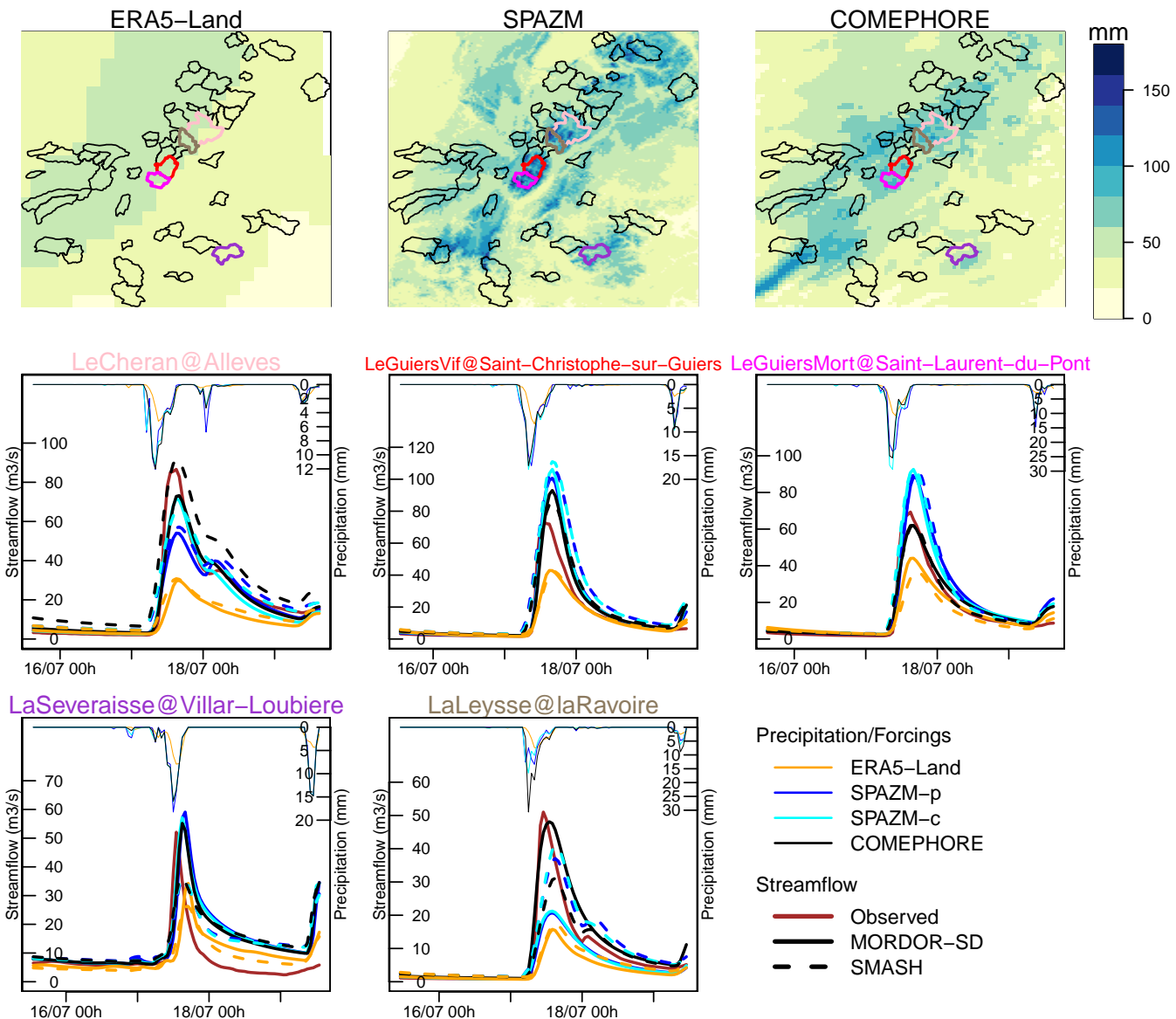


Figure S21. Cumulative amount of precipitation 24 hours before and after 2011-07-17 06:00 for ERA5-Land, SPAZM and COMEPHORE (top row) and time series of precipitation (thin lines) and streamflow (thick lines) for five catchments which have reached the highest observed peak flows for this event (middle and bottom rows).

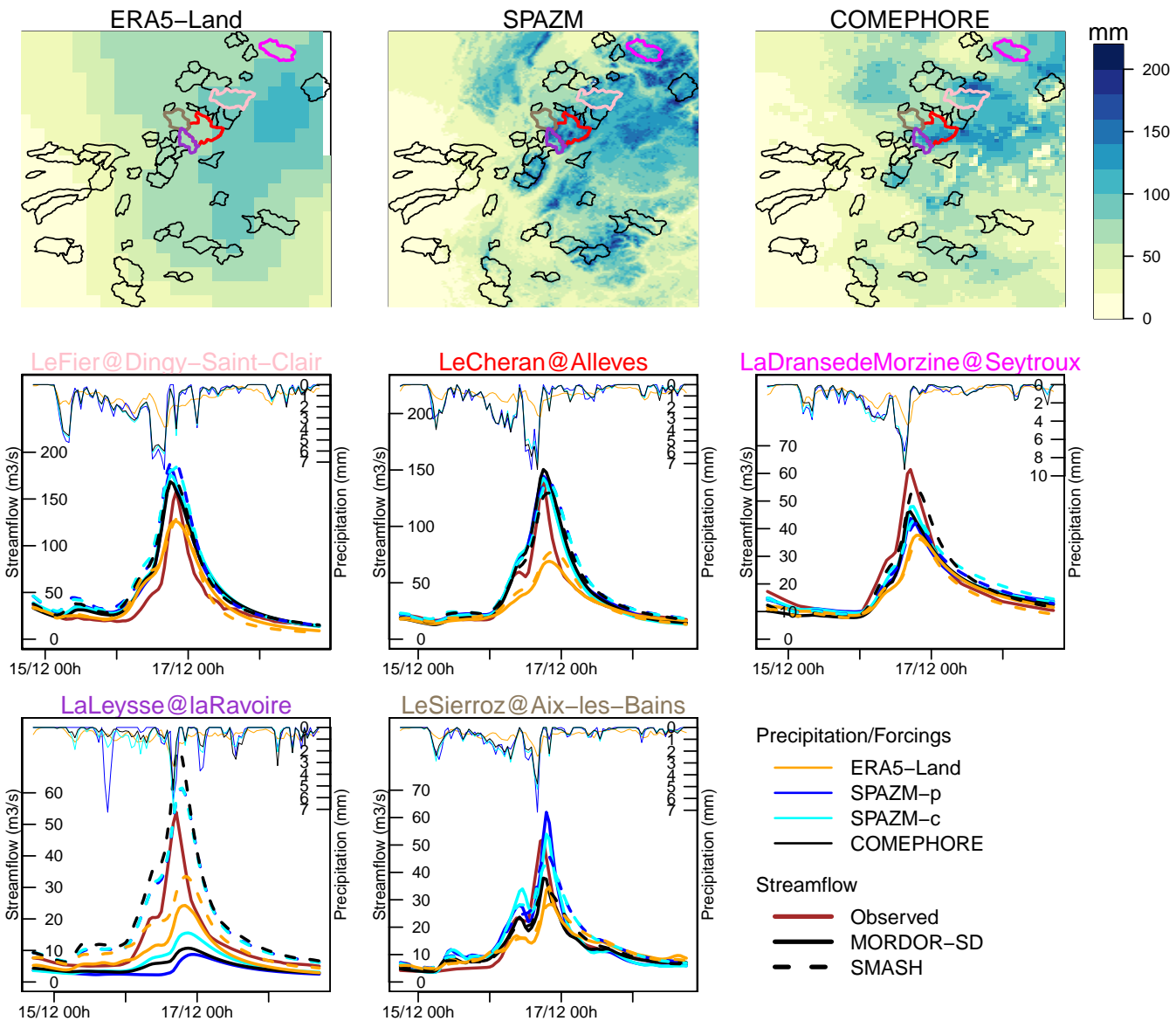


Figure S22. Cumulative amount of precipitation 24 hours before and after 2011-12-16 06:00 for ERA5-Land, SPAZM and COMEPHORE (top row) and time series of precipitation (thin lines) and streamflow (thick lines) for five catchments which have reached the highest observed peak flows for this event (middle and bottom rows).

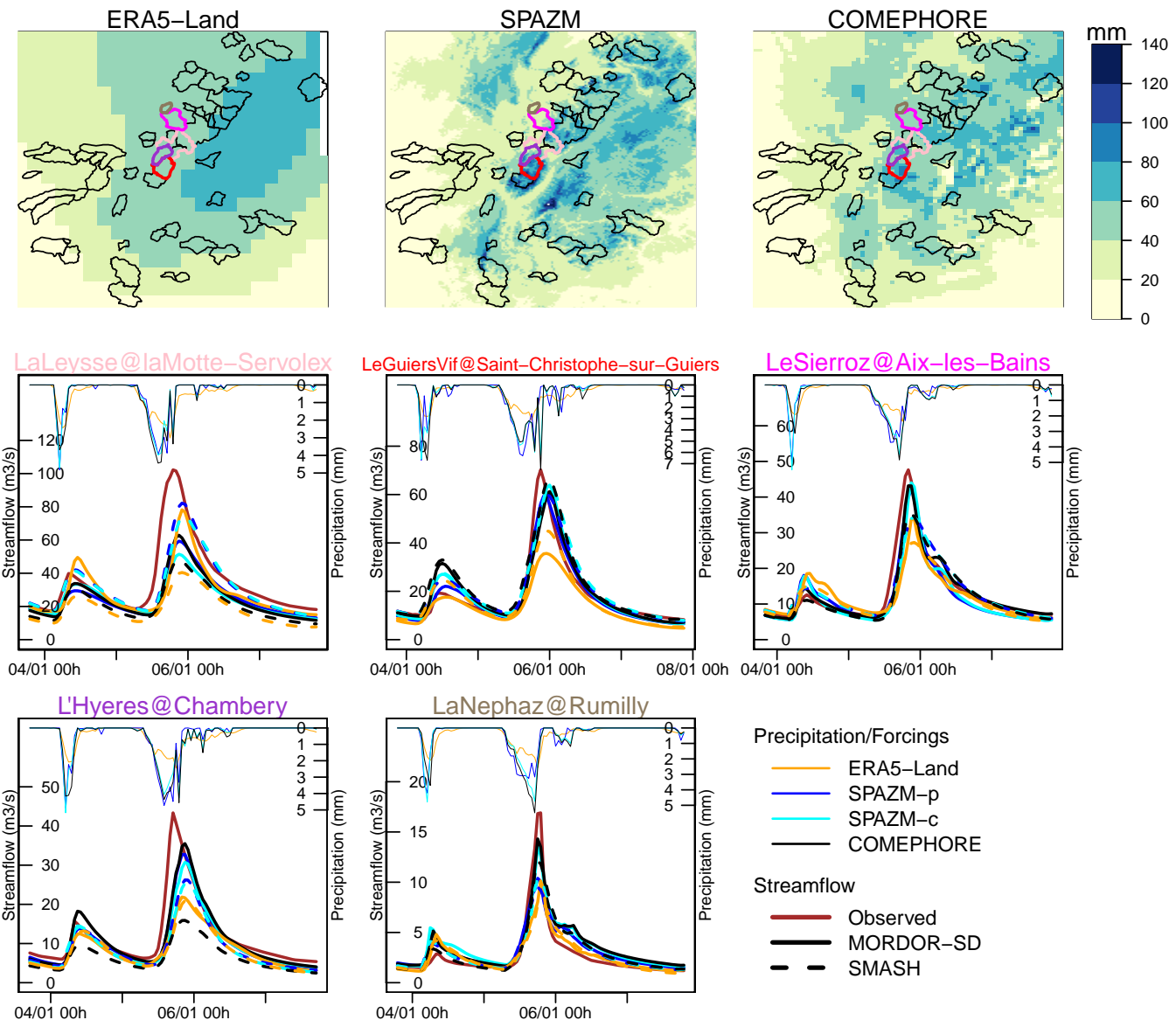


Figure S23. Cumulative amount of precipitation 24 hours before and after 2012-01-05 06:00 for ERA5-Land, SPAZM and COMEPHORE (top row) and time series of precipitation (thin lines) and streamflow (thick lines) for five catchments which have reached the highest observed peak flows for this event (middle and bottom rows).

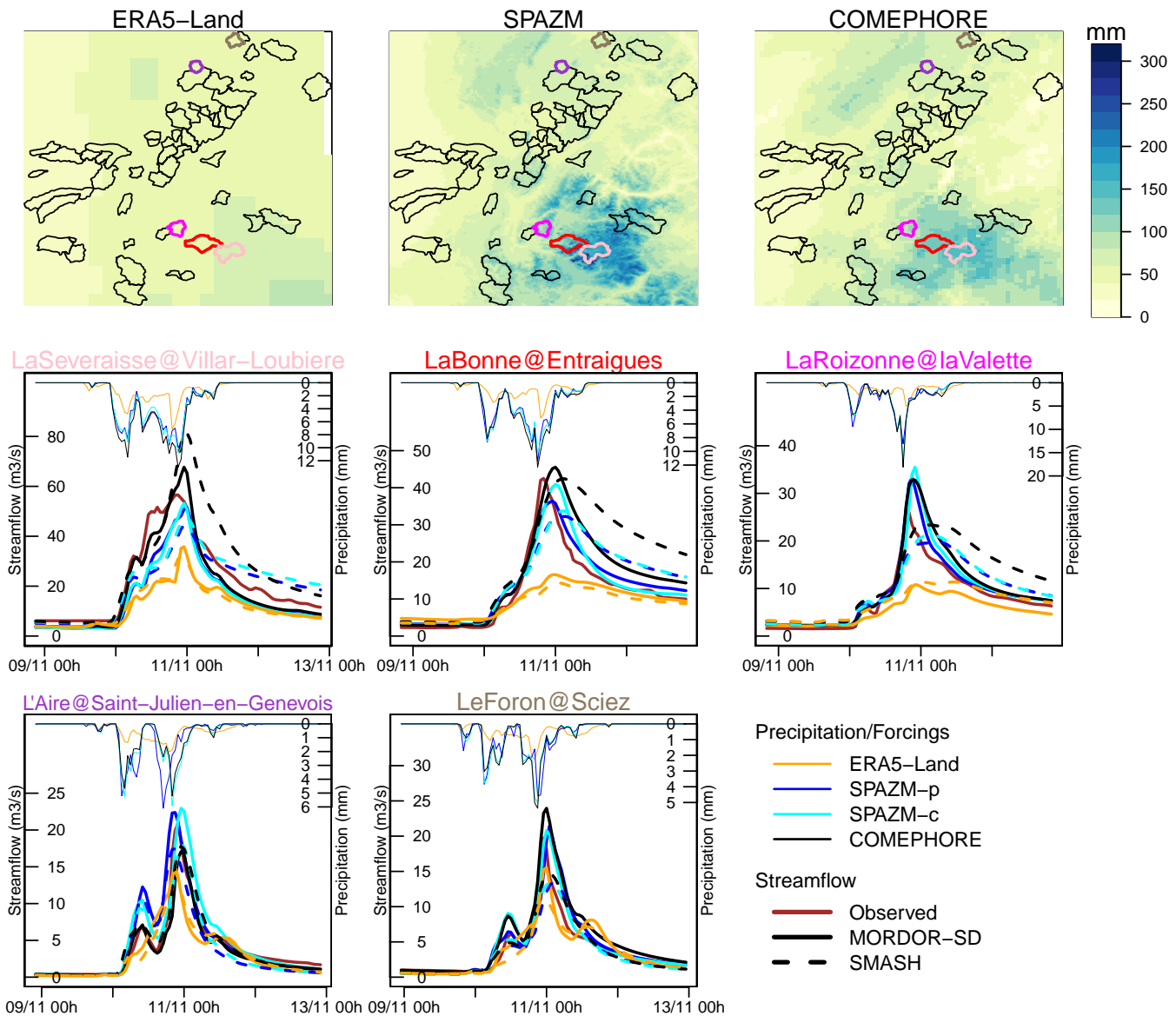


Figure S24. Cumulative amount of precipitation 24 hours before and after 2012-11-10 06:00 for ERA5-Land, SPAZM and COMEPhORE (top row) and time series of precipitation (thin lines) and streamflow (thick lines) for five catchments which have reached the highest observed peak flows for this event (middle and bottom rows).

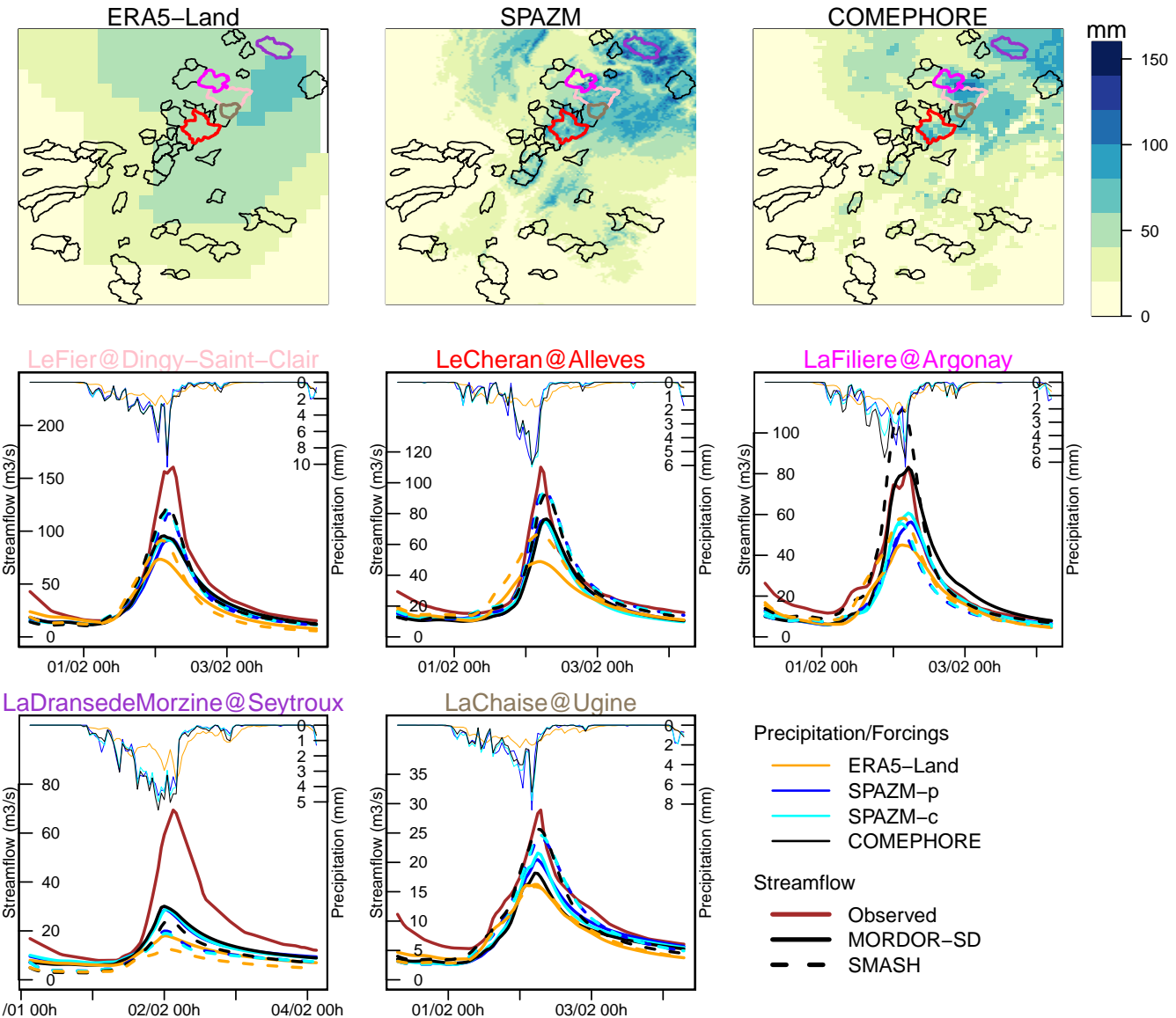


Figure S25. Cumulative amount of precipitation 24 hours before and after 2013-02-02 06:00 for ERA5-Land, SPAZM and COMEPhORE (top row) and time series of precipitation (thin lines) and streamflow (thick lines) for five catchments which have reached the highest observed peak flows for this event (middle and bottom rows).

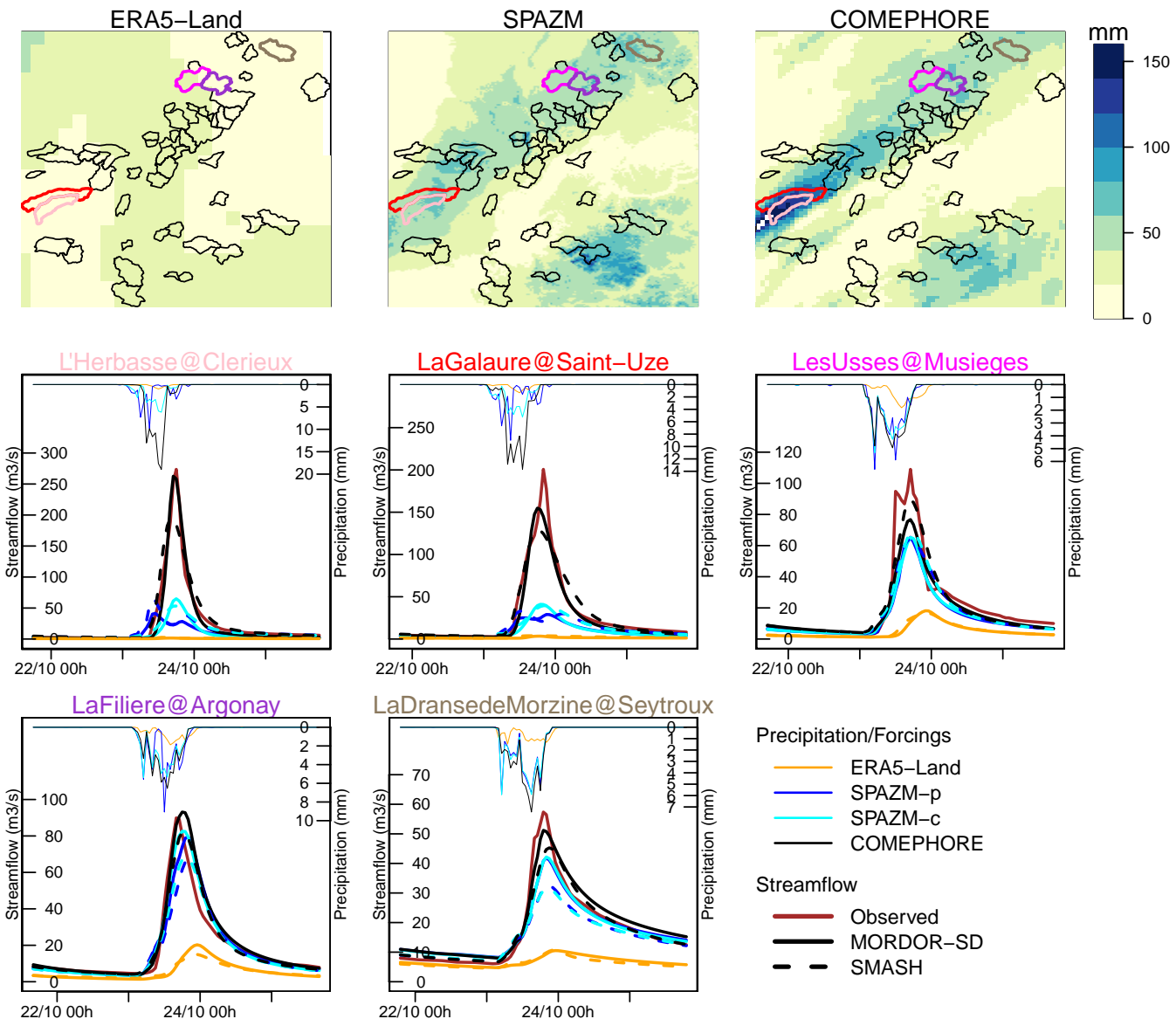


Figure S26. Cumulative amount of precipitation 24 hours before and after 2013-10-23 06:00 for ERA5-Land, SPAZM and COMEPHORE (top row) and time series of precipitation (thin lines) and streamflow (thick lines) for five catchments which have reached the highest observed peak flows for this event (middle and bottom rows).

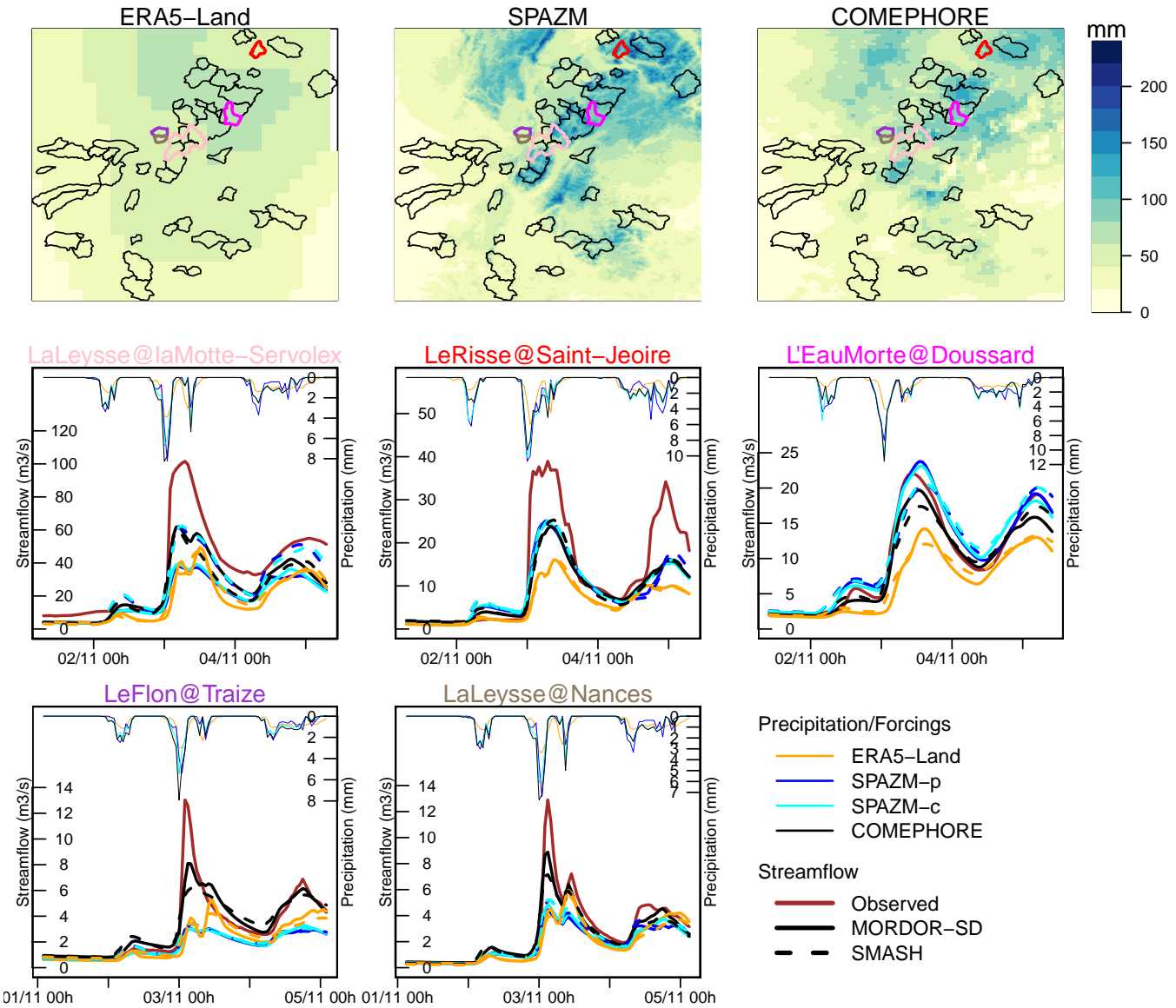


Figure S27. Cumulative amount of precipitation 24 hours before and after 2013-11-03 06:00 for ERA5-Land, SPAZM and COMEPHORE (top row) and time series of precipitation (thin lines) and streamflow (thick lines) for five catchments which have reached the highest observed peak flows for this event (middle and bottom rows).

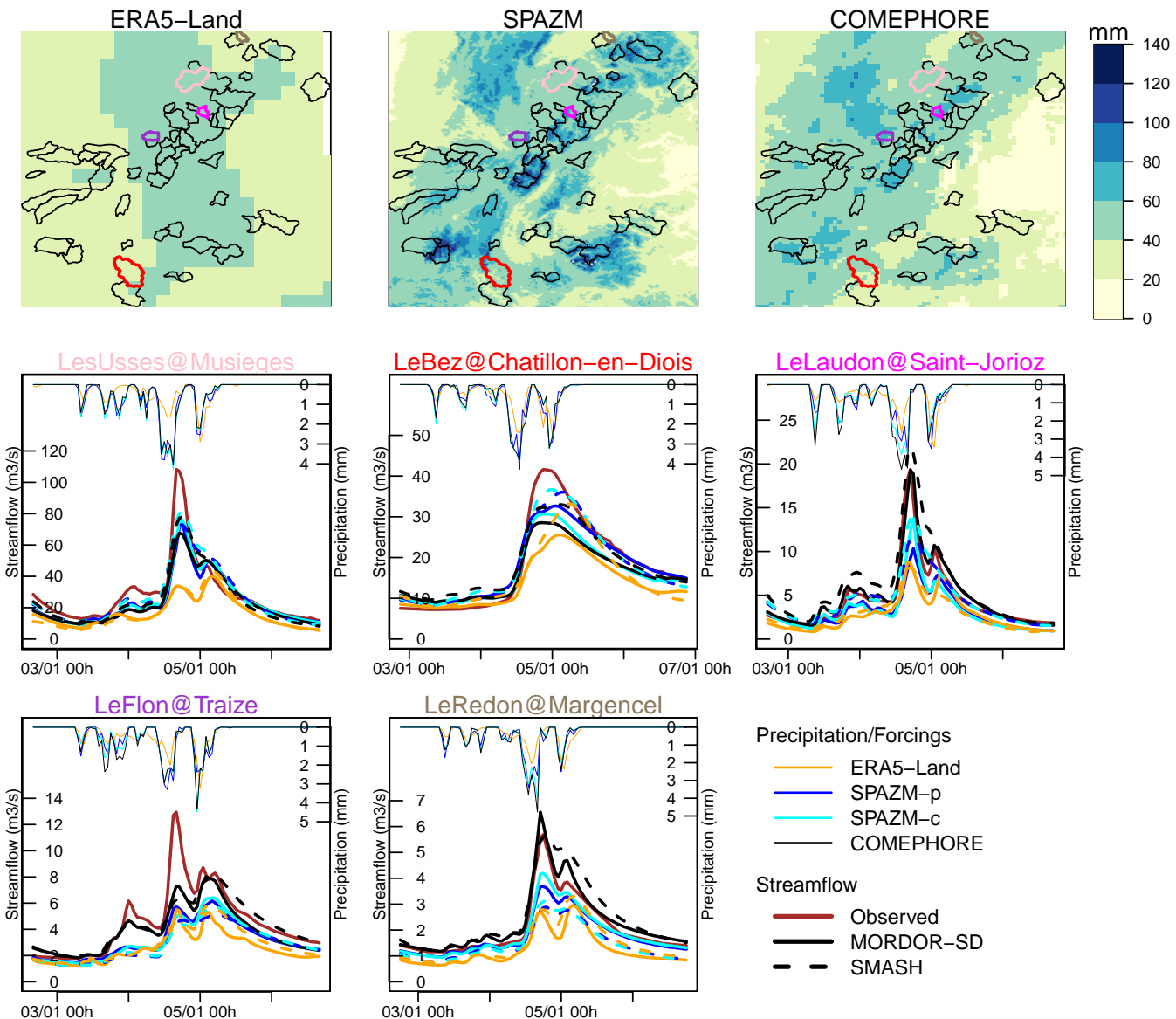


Figure S28. Cumulative amount of precipitation 24 hours before and after 2014-01-04 06:00 for ERA5-Land, SPAZM and COMEPHORE (top row) and time series of precipitation (thin lines) and streamflow (thick lines) for five catchments which have reached the highest observed peak flows for this event (middle and bottom rows).

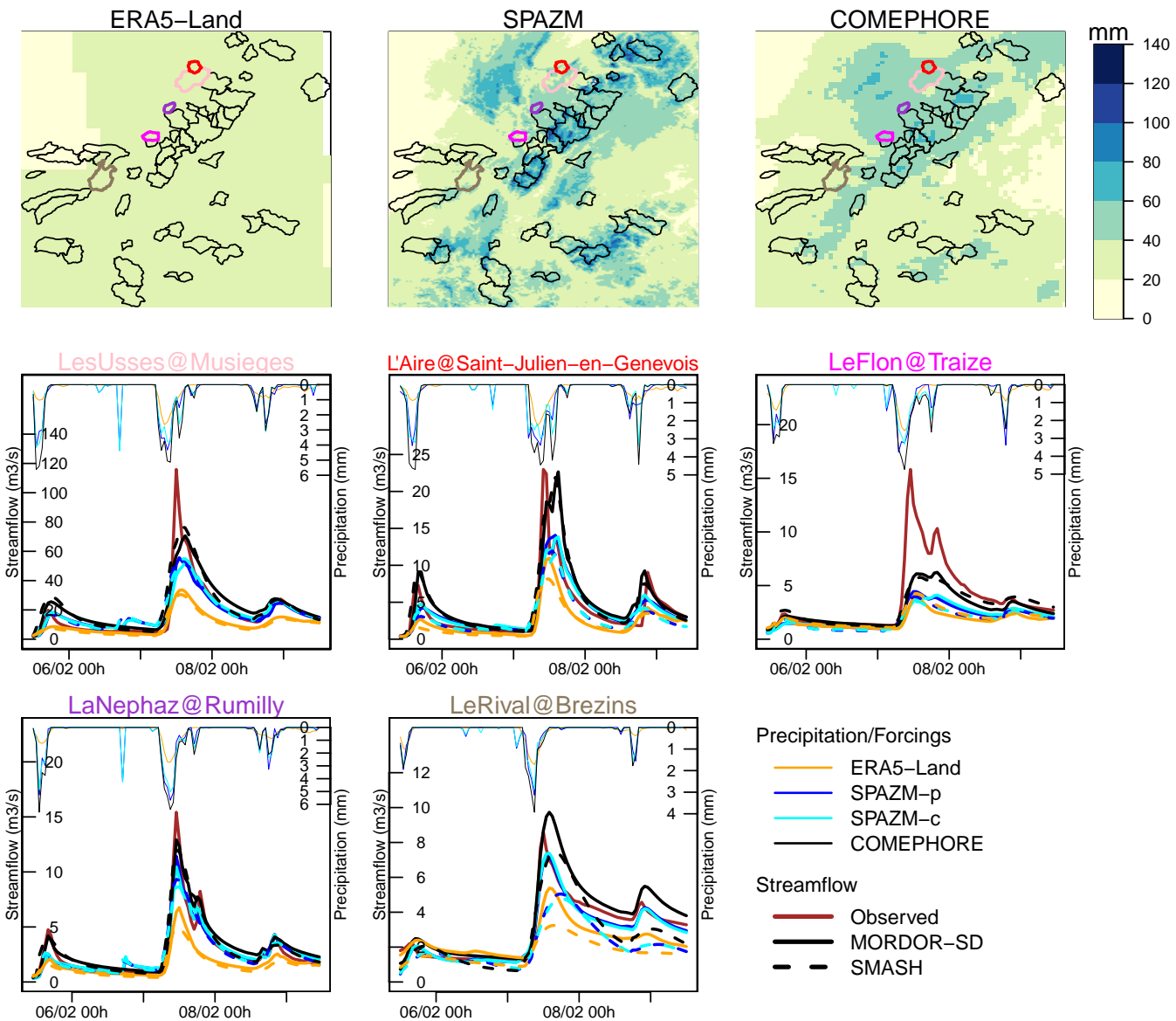


Figure S29. Cumulative amount of precipitation 24 hours before and after 2014-02-07 06:00 for ERA5-Land, SPAZM and COMEPhore (top row) and time series of precipitation (thin lines) and streamflow (thick lines) for five catchments which have reached the highest observed peak flows for this event (middle and bottom rows).

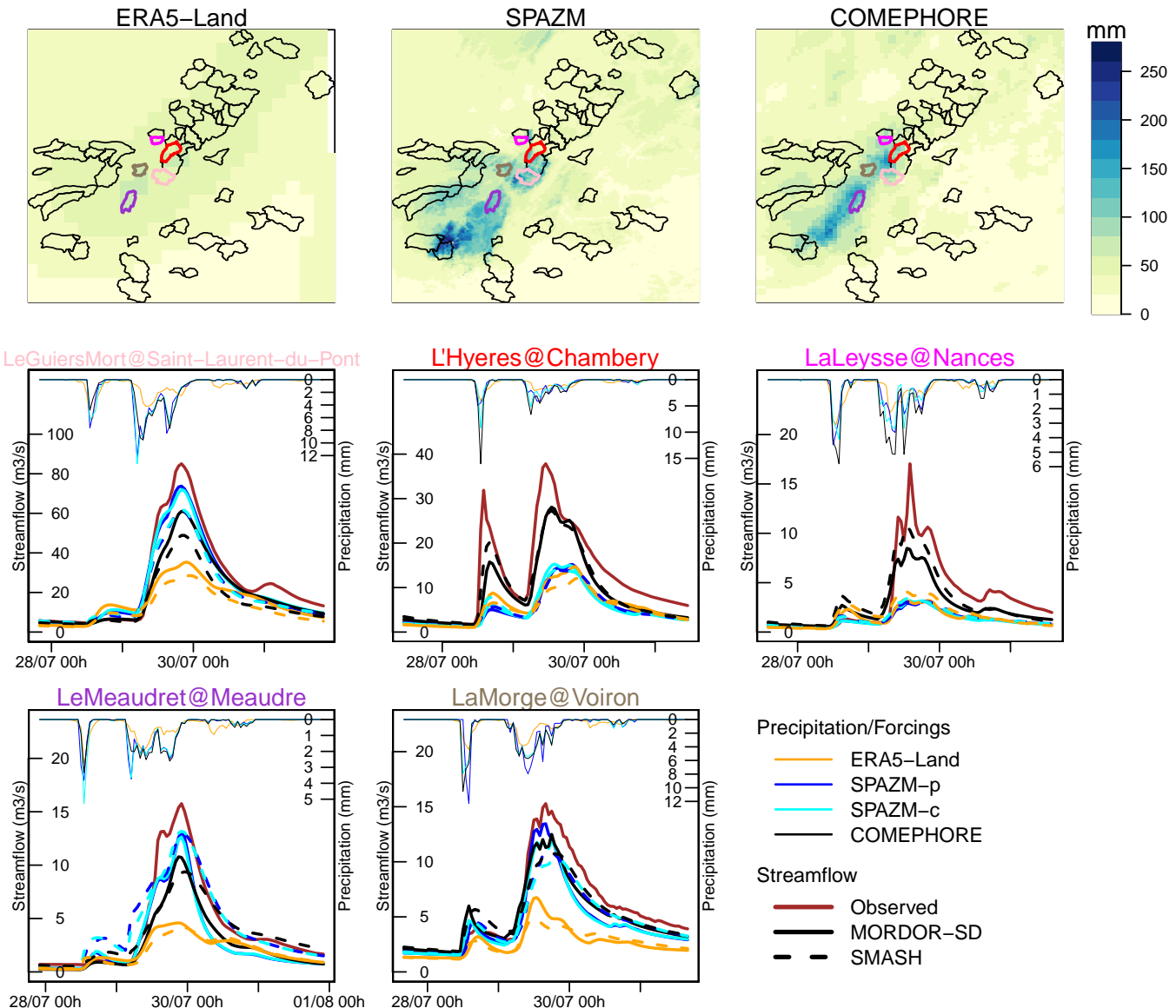


Figure S30. Cumulative amount of precipitation 24 hours before and after 2014-07-29 06:00 for ERA5-Land, SPAZM and COMEPhORE (top row) and time series of precipitation (thin lines) and streamflow (thick lines) for five catchments which have reached the highest observed peak flows for this event (middle and bottom rows).

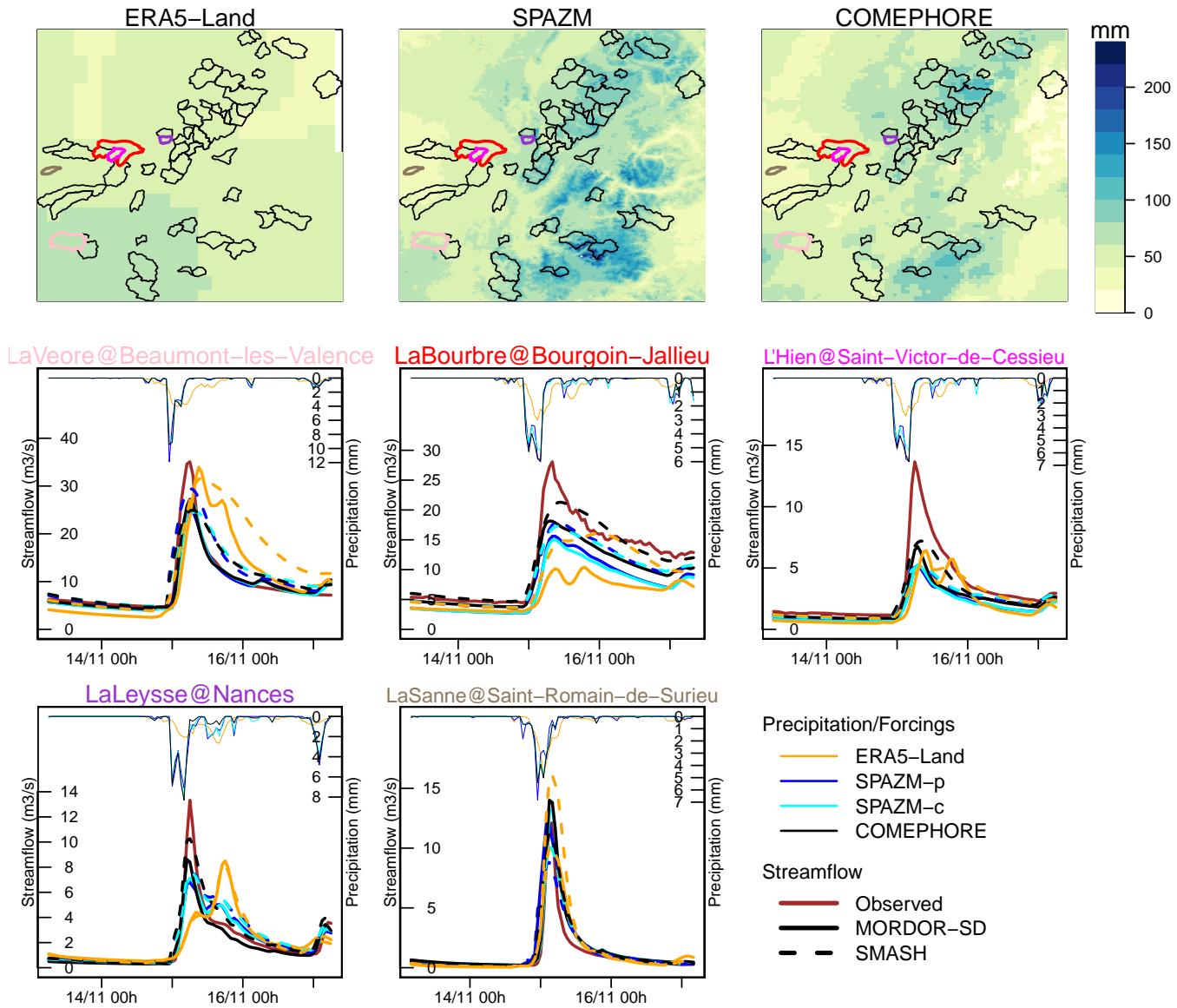


Figure S31. Cumulative amount of precipitation 24 hours before and after 2014-11-15 06:00 for ERA5-Land, SPAZM and COMEPHORE (top row) and time series of precipitation (thin lines) and streamflow (thick lines) for five catchments which have reached the highest observed peak flows for this event (middle and bottom rows).

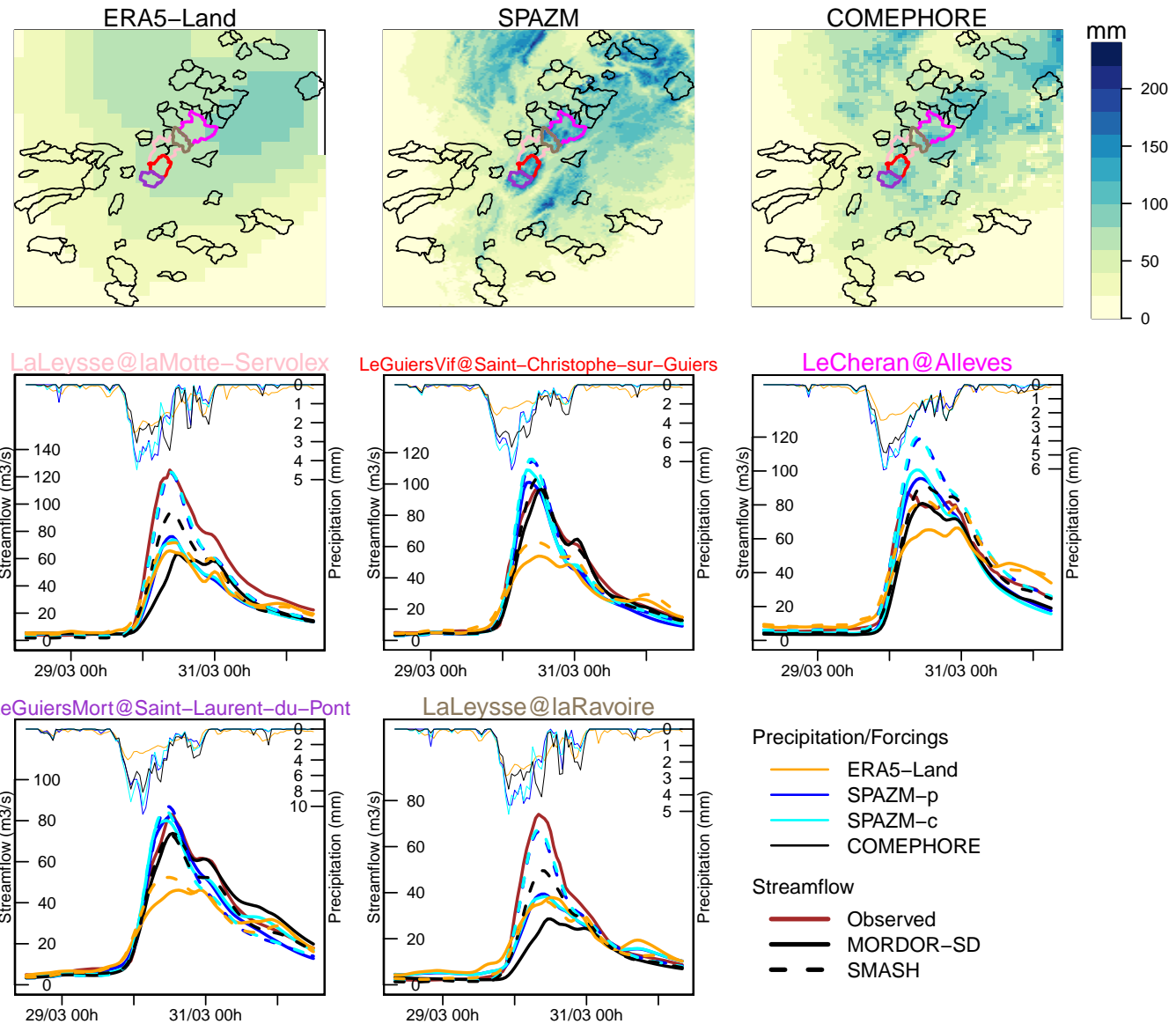


Figure S32. Cumulative amount of precipitation 24 hours before and after 2015-03-30 06:00 for ERA5-Land, SPAZM and COMEPhore (top row) and time series of precipitation (thin lines) and streamflow (thick lines) for five catchments which have reached the highest observed peak flows for this event (middle and bottom rows).

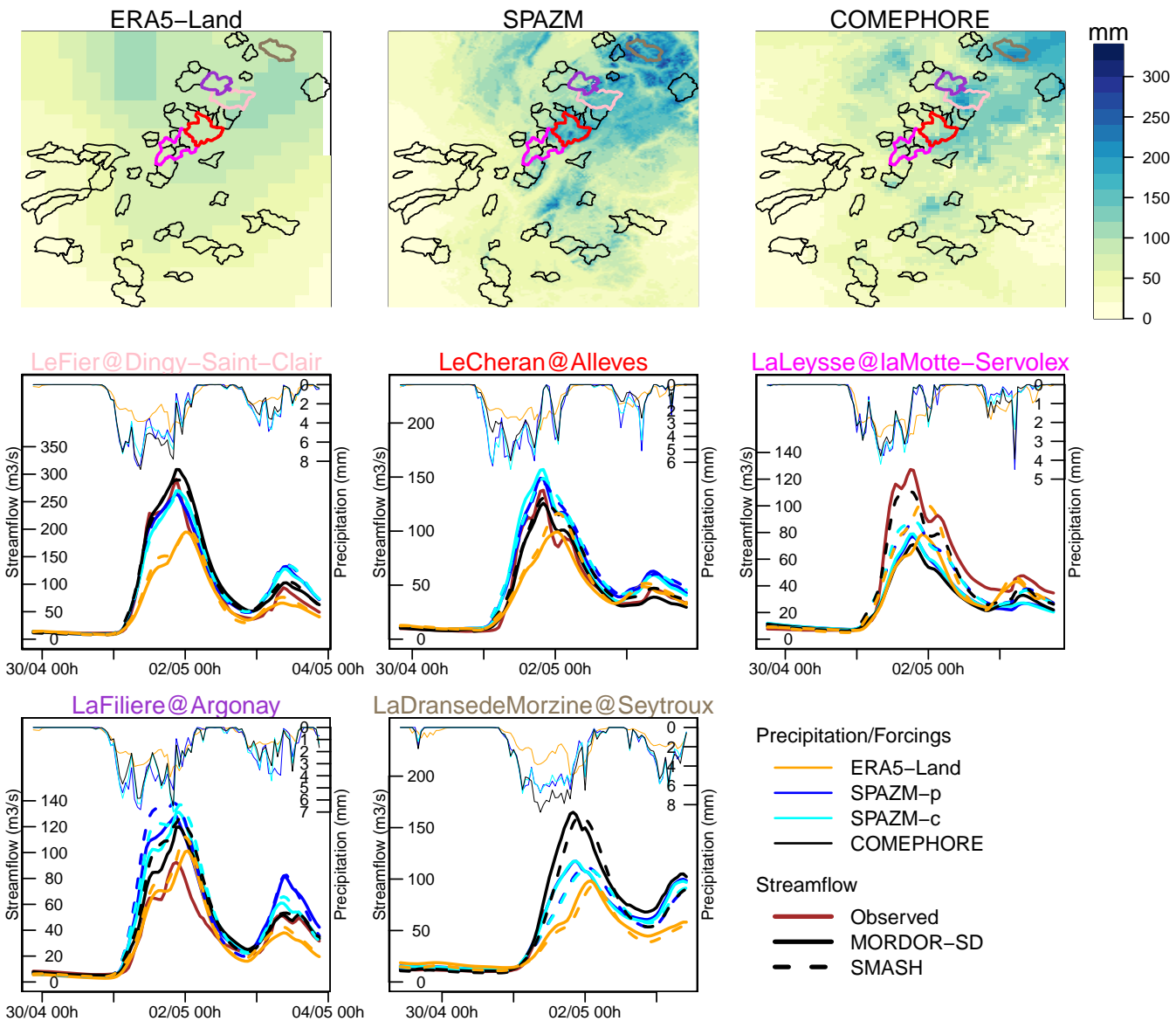


Figure S33. Cumulative amount of precipitation 24 hours before and after 2015-05-01 06:00 for ERA5-Land, SPAZM and COMEPHORE (top row) and time series of precipitation (thin lines) and streamflow (thick lines) for five catchments which have reached the highest observed peak flows for this event (middle and bottom rows).

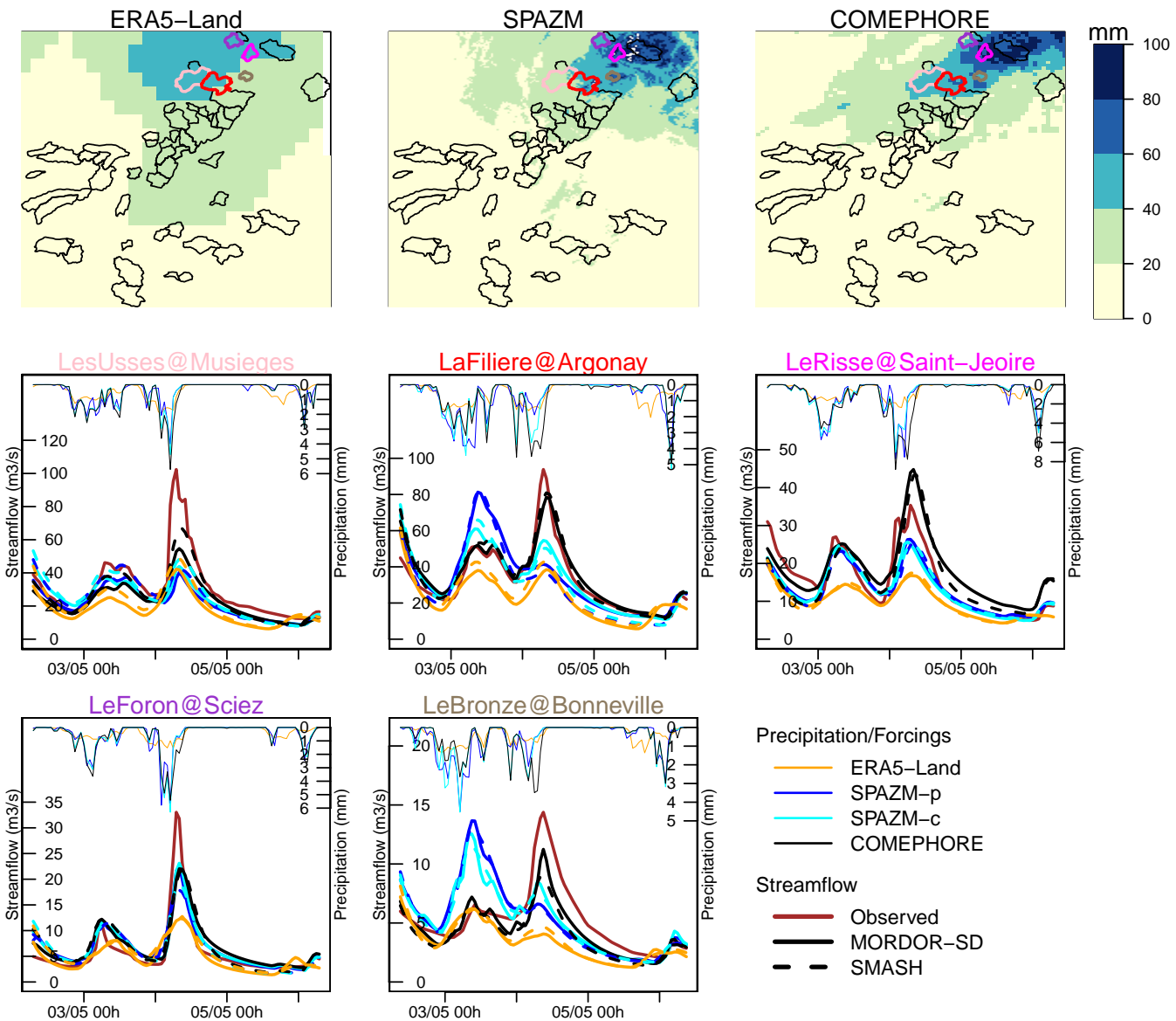


Figure S34. Cumulative amount of precipitation 24 hours before and after 2015-05-04 06:00 for ERA5-Land, SPAZM and COMEPhore (top row) and time series of precipitation (thin lines) and streamflow (thick lines) for five catchments which have reached the highest observed peak flows for this event (middle and bottom rows).

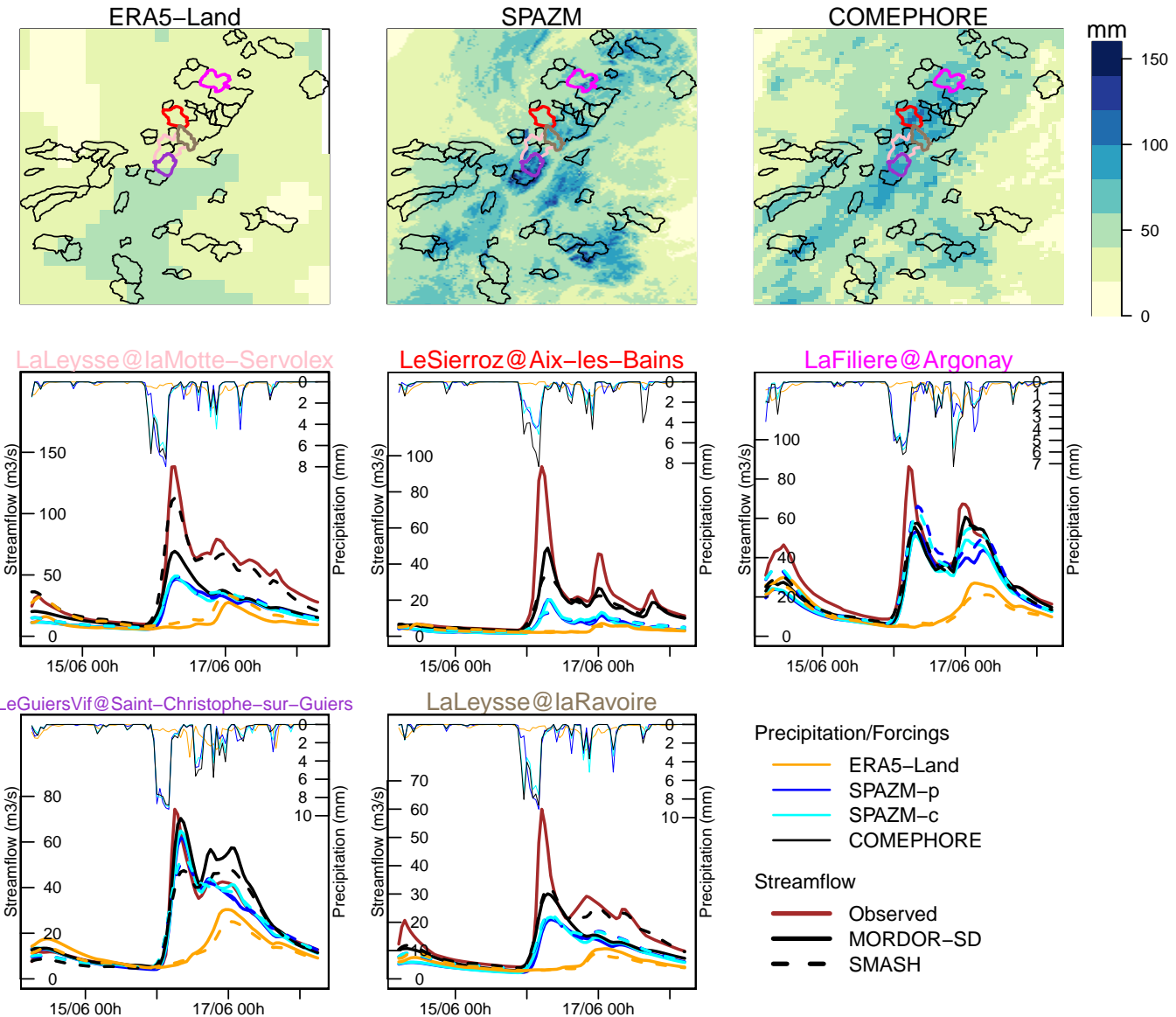


Figure S35. Cumulative amount of precipitation 24 hours before and after 2016-06-16 06:00 for ERA5-Land, SPAZM and COMEPHORE (top row) and time series of precipitation (thin lines) and streamflow (thick lines) for five catchments which have reached the highest observed peak flows for this event (middle and bottom rows).

S6 Maps of the $mNSE(Q)$ in summer and autumn (JJASON)

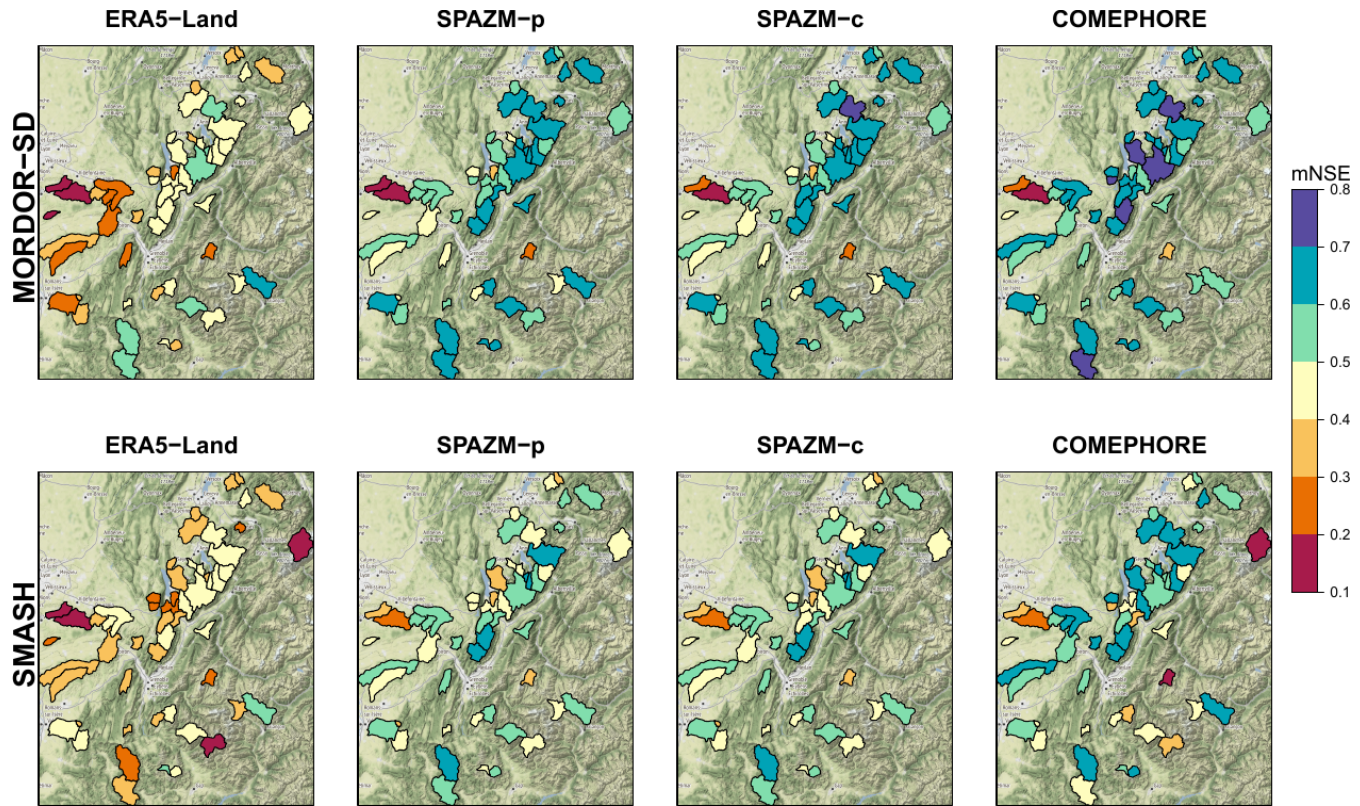


Figure S36. Maps of the $mNSE(Q)$ in summer and autumn (JJASON) obtained with MORDOR-SD (top row) and SMASH (bottom row) and the four types of precipitation forcings. Map © OpenStreetMap contributors 2023. Distributed under the Open Data Commons Open Database License (ODbL) v1.0.

S7 Comparison of performances between periods 1997-2007 and 2008-2017 with COMEPHORE

Figures S37 and S38 shows the differences of performances between periods 1997-2007 and 2008-2017 when COMEPHORE is used as inputs of MORDOR-SD and SMASH, respectively, for different criteria. With MORDOR-SD, a slight improvement of the performances can be noted for the *mNSE* criteria during winter and spring, with larger values of this criteria in about half of the catchments by 0.05-0.1. With SMASH, these differences are more contrasted, and there is no clear improvement/degradation of the performances between the two periods, over all the catchments.

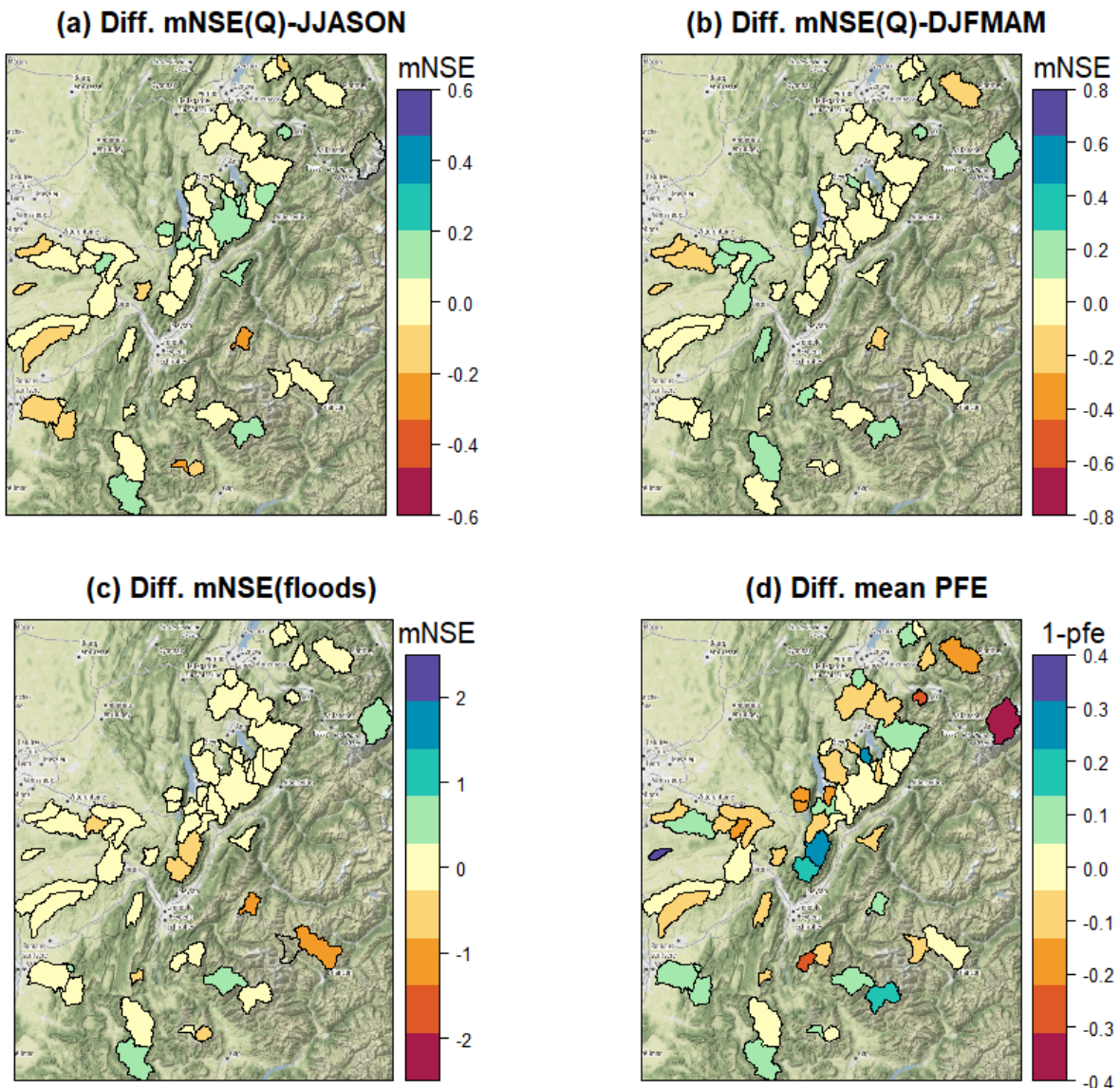


Figure S37. Difference of performances between periods 2008-2017 and 1997-2007 when COMEPHORE is used as inputs of MORDOR-SD. These criteria are positively oriented, which means that positive differences indicate a better performance for the period 2008-2017 than for the period 1997-2007. (a-b) Difference of $mNSE$ criteria for the streamflows Q in DJFMAM and JJASON. (c-d) Difference of $mNSE$ for the 10 largest floods and peak flows error (\overline{PFE}). Map © OpenStreetMap contributors 2023. Distributed under the Open Data Commons Open Database License (ODbL) v1.0.

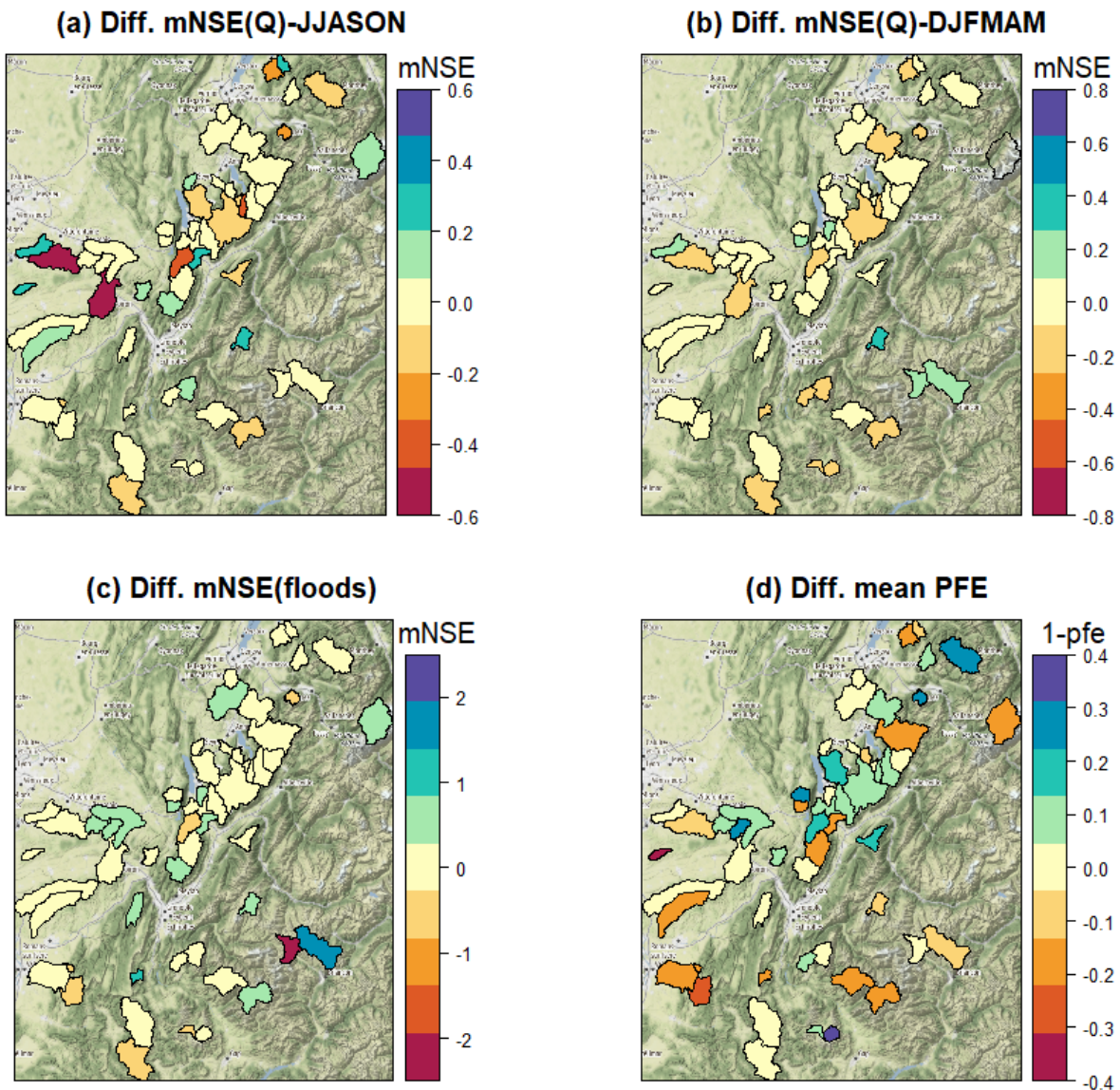


Figure S38. Difference of performances between periods 2008-2017 and 1997-2007 when COMEPHORE is used as inputs of SMASH. These criteria are positively oriented, which means that positive differences indicate a better performance for the period 2008-2017 than for the period 1997-2007. (a-b) Difference of $mNSE$ criteria for the streamflows Q in DJFMAM and JJASON. (c-d) Difference of $mNSE$ for the 10 largest floods and peak flows error (\overline{PFE}). Map © OpenStreetMap contributors 2023. Distributed under the Open Data Commons Open Database License (ODbL) v1.0.

S8 Absolute differences between observed and simulated runoff values

Figure S39 shows the differences of mean daily observed and simulated runoff values, expressed in mm/day, obtained with the different reanalysis, and the two hydrological models, in winter and spring (DJFMAM) and summer and autumn (JJASON). For both hydrological models, slight underestimations are obtained in DJFMAM with SPAZM and COMEPhORE, and overestimations in JJASON. These differences are more important with SMASH than with MORDOR-SD.

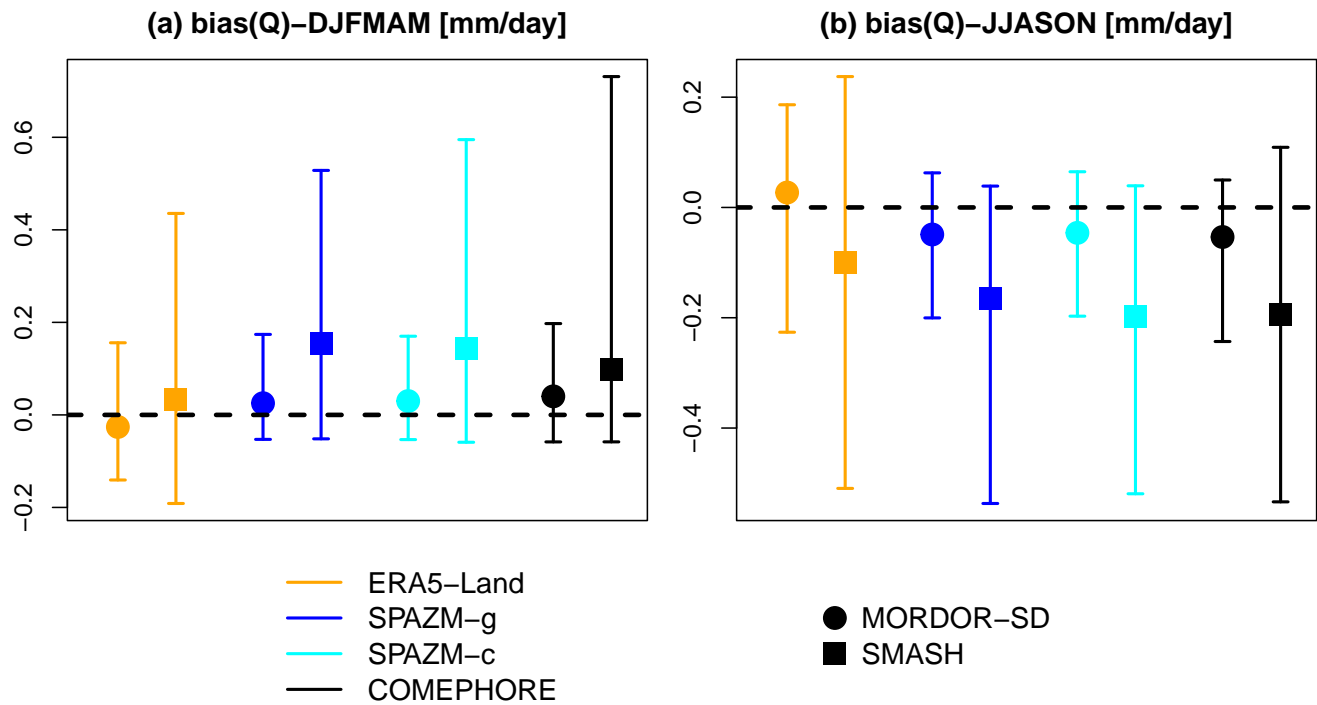


Figure S39. Difference of mean daily observed and simulated runoff, in mm / day, for the different reanalysis and the two hydrological models. (a) Winter and spring (DJFMAM). (b) Summer and autumn (JJASON).

S9 Time series of precipitation and streamflow for the ten largest floods

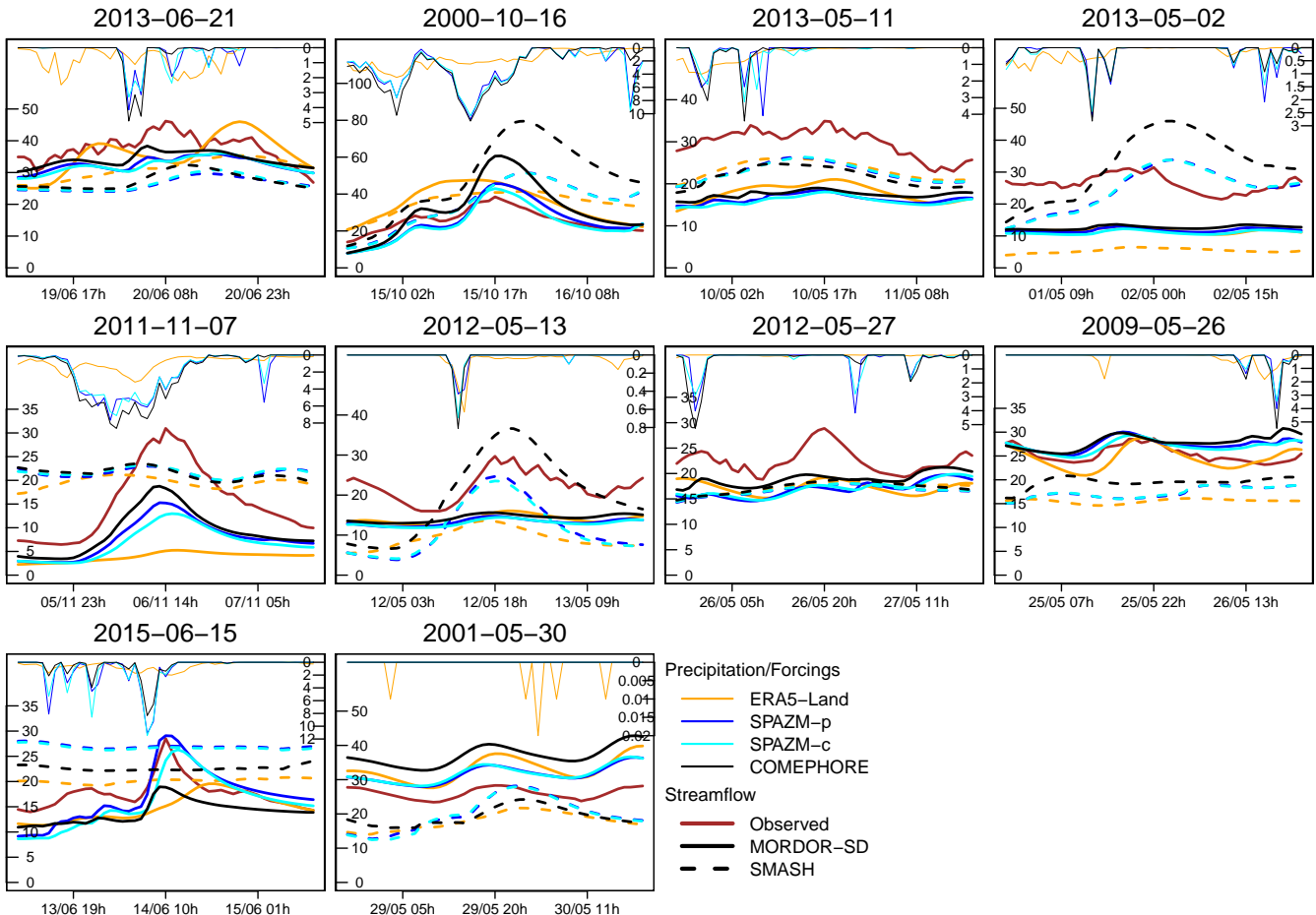


Figure S40. Precipitation and streamflow of the ten largest floods (highest observed peak flows) at LaDurance@Val-des-Pres. Time series of precipitation (thin lines) and streamflow (thick lines) for the different reanalysis.

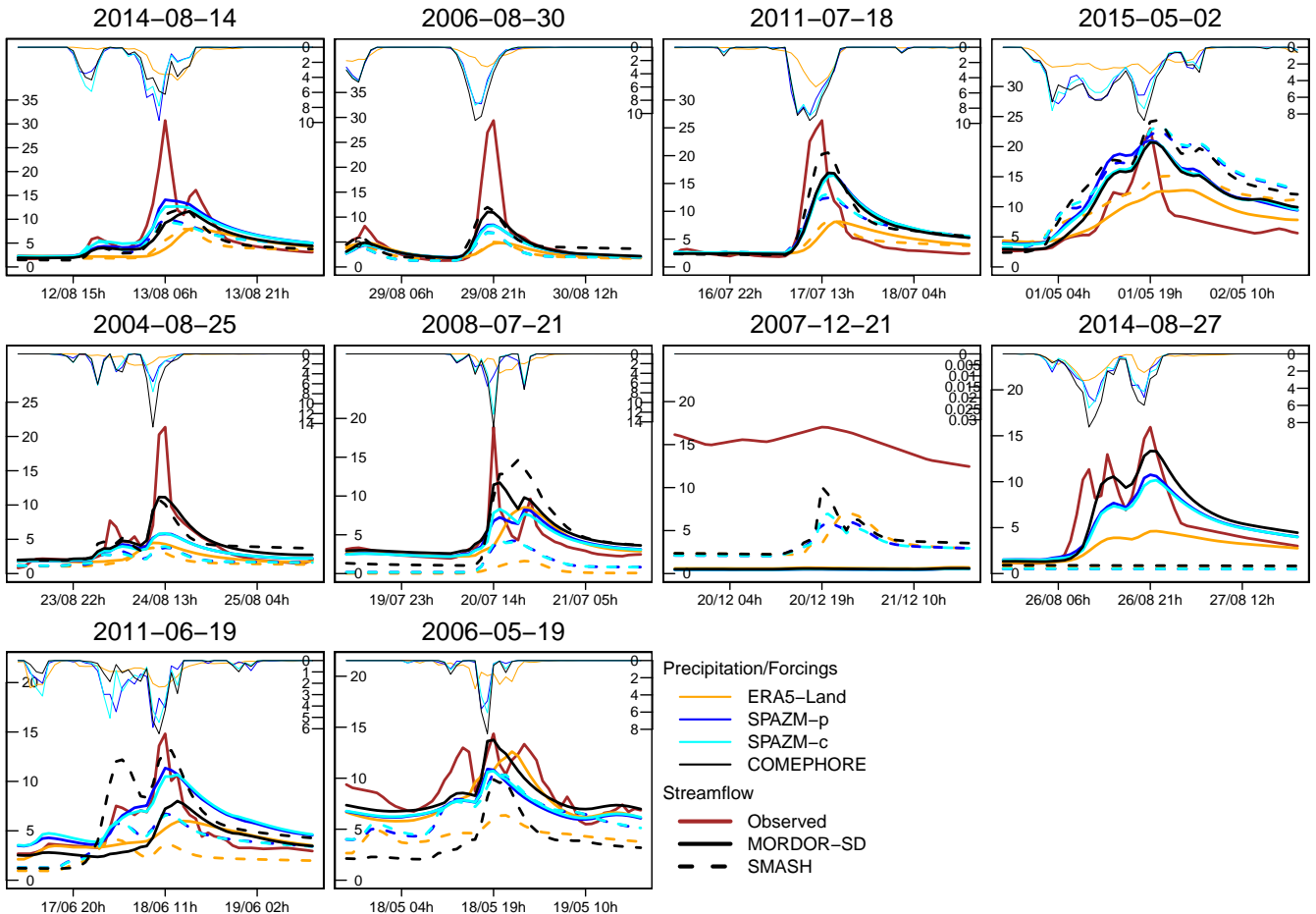


Figure S41. Precipitation and streamflow of the ten largest floods (highest observed peak flows) at L'Arvan@Saint-Jean-d'Arves. Time series of precipitation (thin lines) and streamflow (thick lines) for the different reanalysis.

References

- Breinl, K. and Di Baldassarre, G.: Space-time disaggregation of precipitation and temperature across different climates and spatial scales, *Journal of Hydrology: Regional Studies*, 21, 126–146, <https://doi.org/10.1016/j.ejrh.2018.12.002>, 2019.
- Brugeron, A., Paroissien, J., and Tillier, L.: Référentiel hydrogéologique BDLISA version 2 : Principes de construction et évolutions, Tech. Rep. BRGM/RP-67489-FR, BRGM/OFB, 2018.
- Garavaglia, F., Lay, M. L., Gottardi, F., Garçon, R., Gailhard, J., Paquet, E., and Mathevot, T.: Impact of model structure on flow simulation and hydrological realism: from a lumped to a semi-distributed approach, *Hydrology and Earth System Sciences*, 21, 3937–3952, [https://doi.org/https://doi.org/10.5194/hess-21-3937-2017](https://doi.org/10.5194/hess-21-3937-2017), 2017.
- Jay-Allemand, M., Javelle, P., Gejadze, I., Arnaud, P., Malaterre, P.-O., Fine, J.-A., and Organde, D.: On the potential of variational calibration for a fully distributed hydrological model: application on a Mediterranean catchment, *Hydrology and Earth System Sciences*, 24, 5519–5538, <https://doi.org/10.5194/hess-24-5519-2020>, 2020.
- Oudin, L., Hervieu, F., Michel, C., Perrin, C., Andréassian, V., Anctil, F., and Loumagne, C.: Which potential evapotranspiration input for a lumped rainfall-runoff model?: Part 2—Towards a simple and efficient potential evapotranspiration model for rainfall-runoff modelling, *Journal of Hydrology*, 303, 290–306, <https://doi.org/10.1016/j.jhydrol.2004.08.026>, 2005.
- Perrin, C., Michel, C., and Andréassian, V.: Improvement of a parsimonious model for streamflow simulation, *Journal of Hydrology*, 279, 275–289, [https://doi.org/10.1016/S0022-1694\(03\)00225-7](https://doi.org/10.1016/S0022-1694(03)00225-7), 2003.
- Valéry, A.: Modélisation précipitations – débit sous influence nivale Elaboration d'un module neige et évaluation sur 380 bassins versants, Ph.D. thesis, AgroParisTech, Paris, <https://webgr.inrae.fr/wp-content/uploads/2012/07/2010-VALERY-THESE.pdf>, 2010.
- Wójcik, R. and Buishand, T. A.: Simulation of 6-hourly rainfall and temperature by two resampling schemes, *Journal of Hydrology*, 273, 69–80, [https://doi.org/10.1016/S0022-1694\(02\)00355-4](https://doi.org/10.1016/S0022-1694(02)00355-4), 2003.